1   **Northern Eurasian Heat Waves and Droughts**

2

3   Siegfried Schubert, Hailan Wang[1], Randal Koster, Max Suarez, and Pavel Groisman*

4

5   *Global Modeling and Assimilation Office*
6   *NASA GSFC, Greenbelt, MD*
7
8   ** National Climatic Data Center*
9   *Asheville, NC*
10
11
12
13

14   23 December 2013

15   Revised
16

[1] Also, Science Systems and Applications, Inc

17   **Abstract**

18

19   This article reviews our understanding of the characteristics and causes of northern Eurasian

20   summertime heat waves and droughts. Additional insights into the nature of temperature and

21   precipitation variability in Eurasia on monthly to decadal time scales and into the causes and

22   predictability of the most extreme events are gained from the latest generation of reanalyses and from

23   supplemental simulations with the NASA GEOS-5 AGCM.   Key new results are: 1) the identification

24   of the important role of summertime stationary Rossby waves in the development of the leading

25   patterns of monthly Eurasian surface temperature and precipitation variability (including the

26   development of extreme events such as the 2010 Russian heat wave), 2) an assessment of the mean

27   temperature and precipitation changes that have occurred over northern Eurasia in the last three

28   decades and their connections to decadal variability and global trends in SST, and 3) the quantification

29   (via a case study) of the predictability of the most extreme simulated heat wave/drought events, with

30   some focus on the role of soil moisture in the development and maintenance of such events. A

31   literature survey indicates a general consensus that the future holds an enhanced probability of heat

32   waves across northern Eurasia, while there is less agreement regarding future drought, reflecting a

33   greater uncertainty in soil moisture and precipitation projections. Substantial uncertainties remain in

34   our understanding of heat waves and drought, including the nature of the interactions between the

35   short-term atmospheric variability associated with such extremes and the longer-term variability and

36   trends associated with soil moisture feedbacks, SST anomalies, and an overall warming world.

1. **Introduction**

"*While in western Europe there is continual rain and they complain about the cold summer, here in Russia there is a terrible drought. In southern Russia all the cereal and fruit crops have died, and around St Petersburg the forest fires are such that in the city itself, especially in the evening, there is a thick haze of smoke and a smell of burning. Yesterday, the burning woods and peat bogs threatened the ammunition stores of the artillery range and even the Okhtensk gunpowder factory.*"[2]. This remarkable July 15, 1875 entry in General Dmitry Milyutin's diary reflects not only the fact that Russia suffered from terrible drought and heat in the past, but also a realization long ago that such droughts were at times juxtaposed with cool and wet conditions over Europe. Today, we know this juxtaposition is no coincidence but in fact reflects the unique large-scale atmospheric controls on drought and heat waves affecting much of northern Eurasia. Droughts in Eurasia indeed have a character all their own.

Historical records show that over time the peoples of the Eurasian continent have suffered through numerous heat waves and droughts, events that have impacted the course of battles[3], desiccated important crop lands (thereby inducing famine), produced numerous forest and peat fires, and contributed to thousands of deaths. Gumilev (1960) and Pines (2012) review the pulses of dry and relatively humid periods that have occurred during the past 2 millennia over the entire Great Steppe of northern Eurasia (from Pannonia in the west to Manchzhuria in the east), causing prosperity and decay of ancient states and the migration of nomadic tribes. A compendium of extreme events during the past 1100 years over ancient European Russia (ER), Belarus, and Ukraine (so-called Kiev Rus') is

---

[2] http://therese-phil.livejournal.com/171196.html
[3] The town of Szigetvár, Hungary was under siege by the Turks on 7 August 1566. The main protection of the town was a lake and marshland that normally surrounded it. "Chance however now favored the Turks. A drought had prevailed during the two preceding months, and the terrain surrounding the old town had become so dry, as considerably to facilitate the approach of the enemy." Vámbéry (1886).

58 provided by Borisenkov and Pasetsky (1988), Bogolepov (1922), and Vazhov (1961). Appendix B

59 contains a list of the major droughts and heat waves that have occurred since the late 19th century.

60

61 Droughts continue to have major impacts on northern Eurasian agriculture. As noted in Golubev and

62 Dronin (2004), "Another notable feature of Russian agriculture are the rather large fluctuations in

63 year-to-year yield, which are considerably higher than in any other major grain producing country in

64 the world... These high fluctuations in total cereal production were undoubtedly the result of irregular

65 precipitation." In fact, many of the important early studies on Russian drought and temperature

66 extremes were performed to address their impacts on agriculture in the important growing regions of

67 Povolzhie, North-Caucasus and Central-Chernozem, regions that produce about 2/3 of the Russian

68 food grains (Kleshenko et al. 2005). Kahan (1989) lists some major Russian droughts (based on the

69 work of Rudenko 1958; see also Appendix B) and their agricultural impacts; he notes that the

70 increased impact of natural calamities was in part associated with the expansion of Russian agriculture

71 (mainly grain acreage) toward the south and southeast into the steppes and semi-arid regions

72 characterized by drier climatic conditions. However, these regions are also characterized by fertile

73 soils (chernozem) and have longer growing seasons[4]. This, together with a general increase of grain

74 productivity, appears to have made the severe drought-induced famines of previous years much less

75 likely. For example, the 2010 heat wave and drought over ER (which was so severe that we had to go

76 back to 1092 AD to find an analogue)[5] caused not a famine but did cause a stoppage of grain export

---

[4] For example, when at the end of the rule of Tsar Boris Godunov the Moscow Tsarstvo was struck by a 3-year long famine (1601-1603), cold summers were to blame, most probably related to a catastrophic volcanic eruption of Huaynaputina (Peru) in 1600. At that time the present major grain areas of ER were not plowed and the present region of "sustainable agriculture" in the forested areas of central ER around 55°N simply did not receive summer temperatures sufficient for grain harvests. Ultimately, this famine caused an 8-year-long period of social turmoil, civil war, and invasion by Swedish and Polish marauders, and it ultimately caused a change in the ruling dynasty.

[5] National Yearbooks (Letopisi) prepared by Russian monks since the early 10th century report most important political and environmental events over Kiev Rus' (the area of present northern Ukraine, eastern Belarus, and central part of European Russia). In the 20th century, Letopisi were summed and reanalyzed (Borisenkov and Pasetsky 1988; Barash 1989). Generally, summers over Kiev Rus' in the 11th century were mostly warm and dry. However, on this background, the 1092 summer *was extremely dry*.

77   from Russia. Multiple-year droughts have occurred over the past century, especially in the heartland

78   of the Eurasian steppes (Kahan 1989). Such droughts include the 5-year event (1929-1933) in the

79   Akmolinsk (presently Astana, the capital of Kazakhstan) area. Historically, famines, when they occur,

80   tend to be associated with multiple years of drought (Borisenkov and Pasetsky 1988).

81

82   An interesting and telling aspect of the literature addressing droughts in northern Eurasia is the lack

83   therein of a clear distinction between drought and heat waves. To some extent, this is because

84   summer dryness in this region has two different manifestations: agricultural drought (i.e., soil

85   moisture deficits) and "fire weather" (in the forested areas of northern Eurasia, a prolonged period of

86   hot weather with little or no rainfall) as described in, for example, Nesterov (1949) and Groisman et

87   al. (2007). Agricultural droughts in northern Eurasia also may last for several weeks or even months,

88   particularly under conditions of a short growing season where a complete harvest loss can be caused

89   by a short heat wave that strikes at a critical period of wheat development. Another aspect of droughts

90   in the steppe and semi-desert zones of northern Eurasia are "sukhovey" - an extended period of dry

91   hot winds characterized by intense transpiration and rapid wilting of vegetation (Lydolph 1964).

92   Sukhovey typically emanate from the periphery of anticyclones, bringing in warm and dry air

93   originating   in   the   deserts   of   Africa,   Asia   Minor   and   southern   Kazakhstan

94   (http://en.wikipedia.org/wiki/Sukhovey).   Historically, sukhovey have been a major impediment to

95   large-scale sedentary agriculture in Central Asia (Sinor 1994).   An important point here is that the

96   traditional notions of meteorological (precipitation deficits) and agricultural droughts (soil moisture

---

Moscow Letopis summary for 1092 says: "Huge circle was in the sky in this summer, a drought was so strong that soil was burned and many forest and swamps were set in fire themselves". Letopisi witness: clear skies throughout the entire summer; prolonged period without rainfall; extremely hot weather; fields and pasture "fired out ", and widespread naturally caused forest and peat bog fires (let us recall that at that time wetlands were undisturbed which is opposite to the present state of affairs). In Kiev, in the following autumn and winter more than 7 thousand (of total 50,000) died from starvation. Losses beyond the capital city were (in percent) even higher. This unfortunate development was followed by widespread epidemics.

97 deficits) are perhaps not as relevant nor as clearly separated in northern Eurasia as in other regions of

98 the world.

99

100 The strong link between heat waves and drought in northern Eurasia suggests that we should treat

101 them as different facets of the same phenomena. In fact, many metrics of drought in northern Eurasia

102 involve an explicit temperature criterion; a drought is said to occur, for example, only after a certain

103 minimum number of days with temperatures above a certain threshold (e.g., Selianinov 1928). The

104 strong connection between drought and excessive heat reflects in part the central role of anticyclones

105 in the development of northern Eurasian droughts; the anticyclone inhibits precipitation by blocking

106 or diverting the westerlies and storm systems, and it increases temperature through descending

107 motions (which further inhibit precipitation) and increased insolation associated with clear skies (e.g.,

108 Buchinsky 1976).   Another relevant mechanism involves soil moisture feedback on temperature;

109 reduced precipitation leads to reduced evaporative cooling of the land surface. While multi-year

110 droughts do occur in Eurasia, particularly toward the south of our study area, most droughts have

111 shorter time scales; most severe events[6] occurring across northern Eurasia in fact rarely exceed 50

112 days in duration (Cherenkova, 2007). The north/south differences and east/west differences in

113 drought occurrence reflect the spatially varying influences of the oceans and various air masses

114 (tropical, subtropical, polar) across the continent and the arrangement of Eurasia's major mountain

115 chains.

116

117 The recent extreme heat waves and droughts of 2003 (Europe) and 2010 (Russia) have highlighted the

118 urgency of understanding better their causes and whether or not they are a manifestation of a warming

---

[6] However, as mentioned above , it is enough in this part of the world to have several days of adverse weather during particular periods of cereal growth to cause crop loss. Such short-term events (waves) are much more frequent than long periods of decremented weather.

119 world (e.g., Dole et al. 2011; Trenberth and Fasullo 2012; Otto et al. 2012). While there is

120 agreement on many aspects of such extreme events, including the role of anticyclones, there are still

121 substantial unknowns about their causes and predictability. In particular, we do not yet understand

122 which large scale processes (including climate change, SST, monsoons, links to higher latitudes) may

123 have played a role in making them so exceptional.

124

125 In this paper, we delve into some of the outstanding questions regarding the nature and causes of

126 Eurasian heat waves and droughts, their predictability, and what we can expect in a future warmer

127 world. We focus on northern Eurasia, in particular the region outlined in the Northern Eurasia Earth

128 Science Partnership Initiative (NEESPI, Groisman et al. 2009) – longitudinally, this region extends

129 from 15°E to the Pacific coast, and latitudinally it extends from 40N to the Arctic Ocean coastal zone.

130 The region includes the territory of the former Soviet Union, Fennoscandia, Eastern Europe, Mongolia

131 and north China, though our presentation of the results often extends beyond it in order to provide a

132 more global perspective of relevant teleconnections and physical mechanisms.

133

134 This paper is part of a Global Drought Information System (GDIS) special collection that addresses

135 the causes of drought world-wide. We note that there are separate papers in this collection focusing

136 on drought in large regions bordering and in part overlapping northern Eurasia, including papers on

137 Europe, the Middle East and southwest Asia, and eastern Asia (Seneveratne et al. 2013; Barlow et al.

138 2013; Zhang and Zhou 2013). The interested reader is referred to those papers for more information

139 on those regions. In keeping with the guidelines of the submissions to the GDIS special collection,

140 we will touch on the following topics:

141   i) Drought/heat wave occurrence, metrics, and impacts

142   ii) Key regional circulation features and physical processes

143   iii) Trends

144   iv) Predictability and projections

145   v) Gaps in our understanding

146

147   We begin in Section 2 by discussing the morphology and metrics of droughts and heat waves. Section

148   3 examines the physical mechanisms responsible for their occurrence. Section 4 contains a review

149   and analysis of interannual variability and trends, and Section 5 discusses projections and

150   predictability. A summary is provided in section 6. In addition, two appendices are provided:

151   Appendix A describes the datasets and model simulations used in this study, and Appendix B provides

152   a compilation (based on various sources including research papers and the popular literature) of some

153   of the major droughts and heat waves that have occurred in northern Eurasia since 1875.

154   **2. The morphology and metrics of northern Eurasian heat waves and droughts**

155   *a) Characterizing drought and heat waves*

156   The previous discussion highlighted the adverse impacts of prolonged drought conditions, as well as

157   shorter-period (weeks to months) heat waves and related droughts, on the main agriculture regions of

158   northern Eurasia, with the latter events also playing an important role in the occurrence of "fire

159   weather" in the forested areas of northern Eurasia.   The discussion also emphasized the importance of

160   the interplay between temperature and precipitation variability in the development of droughts.

161   Droughts are ultimately driven by precipitation deficits, and their impacts (e.g., on agriculture) depend

162   on the extent to which they lead to deficits in soil moisture and other water resources important to

163   society.   Temperature increases associated with the precipitation reductions, which can act to

164   exacerbate the drought conditions, can result from reductions in cloudiness; reduced cloud cover over

165 northern Eurasia in summer can warm the surface, since daytime warming is 2-3 times stronger than

166 the nighttime cooling, and the period of daylight is longer than the period of nighttime (Groisman et

167 al. 1999; Tang et al. 2012; Tang and Leng 2012a,b). The temperature increases can also result from

168 reductions in soil moisture, which lead to reduced evaporation and thus reduced evaporative cooling

169 of the surface. Finally, various dynamical processes linked to (for example) the development of

170 persistent anticyclones (the subject of the next section) can act to further reduce cloudiness and

171 precipitation and at times can lead to intense heat waves.

172 Here we look at various measures that highlight and quantify the above aspects of droughts and heat

173 waves over northern Eurasia. A number of different indices are available for consideration. Most are

174 based on joint consideration of precipitation and temperature, with a focus on agricultural applications

175 (e.g., Meshcherskaya and Blazhevich 1997; Kleshenko et al. 2005); examples include the

176 hydrothermal coefficient (HTC, Selianinov 1928) and the dryness index of Ped (1975).

177 Meshcherskaya and Blazhevich (1997) developed a combined drought and excessive moisture index

178 (DM) that takes into account the areal extent of the precipitation and temperature anomalies.

179 Appendix B provides more details on these and several other of the more popular metrics.

180

181 The overall character of northern Eurasian precipitation and temperature variability and its

182 relationship to drought and heat waves is now examined. Figure 1 (left panels) shows the variance of

183 June-July-August (JJA) mean precipitation for the last three decades (1979-2012) as determined by

184 two different reanalyses and from an analysis of station observations. While there are some

185 differences, there is general agreement that the largest precipitation variance over northern Eurasia

186 occurs over European Russia extending eastward along about 55°N – a region for which the maximum

187 rainfall in summer is associated with cyclones from the Atlantic reaching the Yenissey River Valley in

9

188 Central Siberia. Other regions with relatively large precipitation variance are found in the West

189 Caucasus and in the mountainous regions of southeastern Russia/northeast China. Minimum

190 variances are seen in the desert regions east of the Caspian Sea extending to northwestern China and

191 Mongolia.

192

193 While a precipitation deficit is the basic ingredient of drought, the link between the magnitude of such

194 deficits and the presence of drought, at least as defined by established drought indices, is not readily

195 apparent. To make this link quantitative we take as an example the connection of the precipitation

196 deficits with the Ped (1975) dryness index, S_i (the difference between the normalized anomalies of

197 JJA-mean surface temperature and precipitation - see Appendix B for definitions).   The variance of

198 S_i is

199 $$V = 2\,(1 - \rho),\qquad\qquad\qquad\qquad (1)$$

200 where ρ is the correlation between the surface temperature and precipitation. The variance in drought

201 as measured by the Ped (1975) dryness index thus highlights the fact that drought depends on the

202 interplay between precipitation and temperature.   Figure 1 compares the variance field for the drought

203 index (right panels) to that for precipitation (left panels). Note that a comparison of the magnitudes is

204 irrelevant, since the fields have different units; here, we consider only the comparison of spatial

205 patterns. For the dryness index, the largest values (regions with the largest negative correlations

206 between P and T) occur farther south, extending across the main agricultural regions of northern

207 Eurasia, as well as over much of Mongolia and northeast China. Consistent across the three estimates

208 are the relatively large values to the north and east of the Caspian Sea (including northern

209 Kazakhstan), over the Caucasus, and over much of Europe, including the Balkans. In essence, the

210 comparison in Figure 1 shows that standard drought indices do not simply describe the absolute

211   magnitudes of precipitation deficits but, as we shall see in Fig. 2, also reflect the important link with

212   temperature.

213

214   We note that the coefficient of variation (C_v) relates precipitation fluctuations to mean or "normal"

215   climate values – a metric that is in principle[7] perhaps a better measure of precipitation irregularity as it

216   relates to potential impacts on agriculture.   Shver (1976) showed, for example, that while C_v of

217   monthly rainfall totals over Eurasian agricultural areas north of 55°N from May to July are close to

218   0.5, further south C_v gradually increases and in the North Caucasus, southern Ukraine, and northern

219   Kazakhstan reaches values of 0.7 in July and 0.8 in August, indicating the latter regions experience

220   larger swings in precipitation relative to the mean.

221

222   We next turn to the temperature variance. The left panels of Figure 2 show that the variance of the

223   JJA mean is characterized by generally increasing values with latitude, with the largest variance

224   occurring north of Caspian Sea and over the Ural Mountains. While this looks nothing like the

225   distribution of the precipitation variance (Fig. 1, left panels), we have already seen that there are

226   regions where the precipitation and temperature are correlated (Fig. 1, right panels).   We can quantify

227   the extent to which the temperature variability is "explained" by precipitation variability via simple

228   linear regression. The results (left panels of Figure 2) indicate that precipitation variability explains a

229   substantial fraction of the temperature variance over much of southern European Russia and western

230   Siberia (e.g. through evaporative cooling). The similarity to the variance of the Ped index (c.f. Fig. 1,

231   right panels) is not surprising since both measures depend on the correlation between the temperature

232   and precipitation. Furthermore these regions occur in the transition between so-called water-limited

---

[7] In practice this metric is sensitive to bias in the estimates of the mean state.

233 (to the south) and energy limited (to the north) climate regimes (Koster et al. 2006a, Fig. 4a), where

234 land feedbacks are particularly important (Koster et al. 2004). We will look more directly at the

235 impact of soil moisture feedbacks on temperature variability in the context of model simulations in

236 section 3.

237

238 Of course, as mentioned above, cloud cover can also affect temperature variability. In fact, in an

239 assessment of the role of cloud cover and rainfall on the daytime temperature (T_{max}), Tang et al.

240 (2012) showed that for the western half of northern Eurasia (where the major agricultural regions

241 reside), summer cloud cover is negatively correlated with T_{max} and that these correlations are much

242 stronger than those with precipitation.   Tang and Leng (2012b) show that the variance of Eurasian

243 summer T_{max} is better explained by changes in cloud cover than by changes in precipitation at high

244 latitudes and in the middle latitude semi-humid area, while in northern Eurasia the dependence on

245 precipitation is strong only in the Central Asia arid area.

246

247 The above findings suggest that heat waves in Northern Eurasia are influenced by both soil moisture

248 (and precipitation) and circulation (and cloud cover) anomalies, though it is still unclear which plays

249 the more important role. The interactions involved are indeed complex; precipitation deficits can be

250 caused by decreases in cloudiness, and a dry land surface can suppress evapotranspiration and thus

251 inhibit local cloud formation. All said, it seems reasonable to pay significant attention to the

252 atmospheric factors affecting dry weather (at least for heat waves), e.g., the cyclones and anticyclones

253 that control cloud cover over most of the northern extratropics.

254

255 *b) Persistent anticyclones*

256   The key role of anticyclones in generating Eurasian drought and heat waves has important

257   implications for their spatial structures and time scales.   In Eurasia, severe drought conditions in one

258   region (say, European Russia) are at times accompanied by wet and cool conditions to the west over

259   Europe and/or to the east over parts of Siberia. This is suggestive of an east-west wave structure

260   underlying the surface temperature and precipitation anomalies and thus of strong atmospheric

261   controls. Such structures are evident in the analysis of Eurasian heat waves provided by Gershunov

262   and Douville (2008).   They note that "In both model and observations, there is a strong interannual

263   propensity for Far Eastern Europe to be cold during heat wave summers in West-Central Europe. Both

264   recent extreme European heat wave summers of 1994 and 2003 were cold in far-eastern Europe and

265   warm over north-central Siberia, thus exhibiting Eurasian summer temperature wave train conditions

266   typical of large European heat waves." Stankunavicius et al. (2012) carried out an empirical

267   orthogonal function (EOF) analysis of surface air temperature (SAT) and sea level pressure (SLP) for

268   every (2 month) season over Eurasia based on NCEP/NCAR reanalyses for the second half of the 20th

269   century. They found clear evidence of wave structures in the leading modes of SAT variability during

270   early and late summer. Sato and Takahashi (2006) identified a southern Eurasian wave train

271   extending far enough eastward to affect Japan.

272

273   Using NCEP/NCAR reanalysis data, Stefanon et al. (2012), with a clustering approach, identified six

274   major types of European heat waves for the period 1950-2009. The types found include a Russian

275   cluster, a Scandinavian cluster, a western European cluster, and an eastern European cluster, with the

276   temperature anomalies in phase with the anticyclonic (positive 500mb geopotential height) anomalies.

277   They found that drought appears to be a pre-requisite to heat wave occurrence in western and eastern

278   European heat waves (rainfall deficits in southern Europe), but not for the more northerly Russian or

279   Scandinavian heat waves (see Section 3 below).

280

281   *c. The leading modes of surface temperature and precipitation covariability*

282   The above studies on drought and heat wave characteristics suggest that we can effectively quantify

283   hydro-dynamical variability over Eurasia in terms of the *combined* monthly temperature and

284   precipitation variability.   In order to do this efficiently, we employ a rotated[8] empirical orthogonal

285   functions (REOFs) analysis. The basic quantities used in the calculation of the REOFs (the

286   normalized monthly temperature and precipitation fields) are the same as those used in the calculation

287   of the Ped (1975) drought index (Section 2a). We focus here on monthly rather than seasonal means

288   to better capture the variability associated with persistent large-scale atmospheric waves.

289

290   The first REOF (top panels of Fig 3) shows a clear wave structure in both the temperature and

291   precipitation, with anomalies of alternating sign spanning Eurasia (both across the north over Siberia

292   and to the south into China). The greatest temperature loading (shown here as positive) is centered on

293   European Russia (the European Plain) west of the Ural Mountains. The associated precipitation

294   loadings have negative values on the southeastern quadrant of the main warm anomaly (just north of

295   the Caspian Sea), suggestive of a dynamical link between the temperature and precipitation anomalies.

296   Positive values for precipitation occur over central Europe, Scandinavia, northern Siberia, and

297   mountains of Central Asia. The corresponding time series of the leading REOF (referred to as the

298   rotated principal component, or RPC) in Figure 4 show that this pattern is associated with a trend

299   towards more positive values over the last thirty years; it thus appears to have played an important

300   role in the Russian heat wave of 2010 (relatively large positive values for June, July and August).

---

[8] Rotation (Richman 1986) acts to spatially localize anomalies, and has been found by the authors to produce more physically realistic patterns of variability compared with unrotated EOFs. We note that the REOF methodology has no inherent tendency to produce wave structures, in fact, the localization would tend to de-emphasize connections at large distances.

14

301

302   The second REOF again shows a wave structure, with the largest loading in the temperature field just

303   east of the Urals, indicating an east-west phase shift with respect to the first REOF. Positive values

304   also occur over southern Europe, while negative values occur over Scandinavia, northeastern Europe,

305   and much of eastern Asia. The associated precipitation loadings show negative precipitation

306   anomalies just to the east of the Ural Mountains (again on the southeastern quadrant of the main

307   positive temperature anomaly) and over much of Europe, while positive anomalies stretch from

308   Scandinavia southeastward across Kazakhstan, Mongolia and China. The associated RPCs show that

309   this pattern was very pronounced in August of 2003, during the height of the 2003 European heat

310   wave. We note that the first REOF was also very pronounced (negative) in 2003 though this occurred

311   in June of that year at the start of the heat wave. The associated RPC shows no clear trend in the last

312   three decades (Fig. 4).

313

314   REOFS 3-5 are also characterized by wave structures, with the maximum positive temperature

315   anomalies centered just east of the Caspian Sea, just north of Mongolia, and over northern Europe,

316   respectively. REOF 3 differs somewhat from the others in that it is indicative of a more southerly

317   wave path. In all three cases, the main negative precipitation anomalies are either in phase or slightly

318   to the east/southeast of the main positive temperature anomalies. The associated RPCs (particularly

319   RPC3 and RPC4) indicate a change towards more positive values after about 1995.   We will come

320   back to the trends in Section 4. In the following section, we focus on the mechanisms responsible for

321   such wave structures.

322

323   **3. Physical Mechanisms**

324   *a. A Review*

325   As mentioned in the previous section, it has long been recognized that persistent anticyclones play a

326   fundamental role in the generation of drought and heat waves over northern Eurasia. Buchinsky

327   (1976) summarizes some of the key aspects of droughts in the central part of European Russia and the

328   Volga region, noting that over 70% of them are associated with persistent anticyclones that act to

329   disrupt the predominantly zonal flow and eastward progression of weather systems. He notes that

330   these are primarily Arctic anticyclones that advance from the Barents or even the Kara Sea and

331   become stationary over the plains. Similarly, the work of Selianinov (1928) and others, as

332   summarized in Kleshenko et al. (2005), showed that drought in the arid regions of Russia and other

333   Commonwealth of Independent States (CIS) regions results from the penetration of anticyclonic air

334   masses from the Artic. They note that these anticyclones can act in concert with anticyclones at the

335   southern (40-50°N) and high (approx. 75°N) latitudes. The former become more important further to

336   the west where, for example, Ukraine is impacted by the Azores high. They note that most often the

337   Arctic and Azores intrusions are combined in the Lower Volga and the Southern Yuzhny Ural, leading

338   to pronounced drought conditions.

339

340   Similarly, eastern Europe (e.g., Poland) periodically experiences drought related to a persistent

341   stationary anticyclone (an east European high) that joins with the Azores anticyclone via central

342   Europe (Farat et al. 1998). As noted by Golubev and Dronin (2004) "An especially strong drought

343   takes place when an anticyclone is fed by an air mass from an Azores anticyclone moving in from the

344   West. Moving across Europe, the air mass loses its humidity and reaches European Russia completely

345   dry (Protserov, 1950). The droughts resulting from these large scale atmospheric processes usually

346   cover vast territories of Russia, including the Northern Caucasus, the Middle and Low Volga basin,

347   the Urals, and periodically spread over the central chernozem region and even the northern regions of

348   European Russia. For example, the drought of 1946 covered 50 percent of total agricultural land of the

349   USSR. As a result, the scale and consequences of droughts can be catastrophic for the country."

350

351   The physical mechanisms that determine the persistence and scale of the northern Eurasian

352   anticyclones are still not well understood, though atmospheric blocking has long been considered

353   important. Studies of blocking that focus on the Atlantic and impacts on Eurasia go back to Obukhov

354   et al. (1984) and a number of earlier studies reviewed therein. That study in particular reviewed

355   various potential mechanisms of blocking, including those linked to orography and the instability of

356   the Polar Jet, and it emphasized atmospheric blocking as a precondition for drought in summer, with

357   both the downward movement of air within the associated anticyclone (acting to heat and dry the air)

358   and the blocking of the westerlies (inhibiting the inflow of moisture from the west) contributing to the

359   drought conditions.   More recently, Nakamura et al. (1997) contrasted Pacific and Atlantic blocking

360   events and found that incoming wave activity associated with a quasi-stationary Rossby wave train is

361   of primary importance in the development of blocking over Europe, while the forcing from synoptic

362   scale transients is key for the development over the North Pacific.

363

364   In addition to blocking, a number of other large scale modes of variability can affect northern Eurasia

365   on weekly to monthly time scales. The important role of the Northern Annular Mode (NAM) for

366   Eurasian climate has been documented in numerous studies (e.g., Thompson and Wallace 2001).

367   While many studies have focused on the winter season, others have documented the impact of the

368   NAM on variations in land surface phenology such as the start of the growing season and the timing

369   of the peak NDVI over northeastern Russia (e.g., De Beurs and Henebry 2008). Rocheva (2012)

370   linked the persistent 500mb height anomalies over European Russia and western Siberia to the East

371   Atlantic/Western Russia (EA/WR) and Scandinavian (SCA) patterns of variability, respectively, from

372   May through July – patterns that are still not well understood.

373

374   Bothe et al. (2003) linked drought over Tibet to a Eurasian wave train that spans Eurasia from

375   Scandinavia to the South China Sea. They associated the development of the wave to strong

376   anticyclonic activity over northern Europe/Scandinavia, which in turn is supported by anomalous

377   transient eddy activity associated with the North Atlantic storm track.   Ding and Wang (2005)

378   identified a wave number 5 summertime circumglobal teleconnection pattern confined to the summer

379   jet wave guide with significant impacts on interannual (and intraseasonal – Ding and Wang 2007)

380   temperature and precipitation variations over much of Eurasia and North America, apparently

381   maintained by heat sources associated with the Indian monsoon. Schubert et al. (2011) examined the

382   role of stationary Rossby waves on intraseasonal summertime variability in the Northern Hemisphere

383   extratropics and showed that many of the extreme events, including the 2003 European and 2010

384   Russian heat waves, are associated with a particular recurring Eurasian stationary wave pattern that

385   affects much of the northern Eurasian continent. This, along with other summertime wave structures,

386   were found to be primarily forced by sub-monthly vorticity transients, though it was also found that

387   the waves do at times contribute substantially to the seasonal mean anomalies, suggesting some

388   impact from other longer-term (e.g. SST) forcing.

389

390   Uncertainties about the causes of persistent northern Eurasian anticyclones result from limitations in our

391   understanding of the basic dynamical mechanisms involved and from uncertainties about the impact of

392   global warming, especially in regard to the occurrence of some of the most extreme events (e.g., Dole et al.

393   2011; Schneidereit et al. 2011; Lau et al. 2012; Galarneau et al. 2012; Trenberth and Fasullo 2012; Lupo et

394   al. 2012). On the one hand, for example, Dole et al. (2011) emphasized the important role of internal middle

395   latitude atmospheric dynamics in producing an intense and long-lived blocking event and associated

396   anticyclone (producing the warmest July since at least 1880 in western Russia), and they concluded that

397   neither human influences nor slowly varying ocean boundary conditions contributed substantially to the

398   magnitude of the event.   They also stated that "severe drought occurred with the Russian heat wave, making

399   it likely that land surface feedbacks amplified this heat wave's intensity." Trenberth and Fasullo (2012), in

400   contrast, linked the unusual anticyclone to the development of a large-scale Rossby wave train – suggesting

401   that the wave train was forced by anomalous convection in the tropical Atlantic and northern Indian oceans.

402   They also argue that the heat wave intensified through the cumulative impact of local land feedbacks, linked

403   to increased greenhouse gases. Lau and Kim (2012) highlighted the role of this wave train in linking the

404   Russian heat wave to the Pakistani floods, with land feedbacks acting to amplify the Russian heat wave, and

405   moisture transport from the Bay of Bengal (associated with the northward propagation of the monsoonal

406   intra-seasonal oscillation) helping to sustain and amplify the Pakistani rains.   They argue that the western

407   Russian blocking event was itself instrumental in forcing the Rossby wave. Galereau et al. (2012)

408   highlighted the importance of circulation around the blocking ridge accompanied by enhanced subsidence in

409   the intensification of the heat wave. They also found that downstream energy dispersion from source regions

410   over the North Atlantic modulated the structure and intensity of the blocking anticyclone over western

411   Russia.

412

413   Schneidereit et al. (2012) argue that a number of factors at several different time scales were at work

414   during the 2010 heat wave. They show that the shift to La Niña conditions modulated the stationary

415   wave pattern, supporting the blocking high over Eastern Europe. Also, they found that a polar Arctic

416 dipole mode projected on the mean blocking high, and that transients acted to maintain it. At 10-60-

417 day time scales they identified three different paths of wave action that also contributed to the

418 persistent blocking conditions.

419

420 While numerous studies have addressed the important role of soil moisture feedbacks in European

421 droughts (e.g., Ferranti and Viterbo 2006; Seneviratne et al. 2006; Fischer etal. 2007; Vautard et al.

422 2007; Zampieri et al. 2009; Stefanon et al. 2012), far fewer studies have focused on soil moisture

423 impacts in the rest of Eurasia.   Cherenkova (2012) examined the precursors to summer drought in the

424 European Territory of Russia, finding that of the five most extensive hazardous droughts that occurred

425 between 1936-2010 (1936, 1938, 1972, 1981 and 2010), three (1936,1938 and 1972) were preceded

426 by dry winters and springs, which created conditions for further drought development in the summer.

427 The 1981 drought was not preceded by a dry winter and spring, and they suggest that this explains the

428 smaller area covered by that drought. The 2010 drought was preceded by a cold winter without

429 precipitation deficits, but they suggested that the cold temperatures did impact the snowmelt and

430 spring soil moisture deficits.   As already mentioned, Lau and Kim (2011) found that the 2010 Russian

431 heat wave was amplified by the underlying extensive region of dry soil conditions.

432

433 Hirschi et al. (2011) examined the relationship between soil moisture, drought, and summer heat for

434 central and southeastern Europe, based on observational indices for 275 station observations. They

435 found that dry soil conditions intensified hot extremes in the southeastern (Romania and Bulgaria)

436 area, especially for the high end of the distribution of temperature extremes, whereas this was not the

437 case for central Europe (Austria and Czech Republic); they further noted while that the former area is

438 characterized by soil moisture-limited evaporation, the latter is characterized by energy-limited

20

439   evaporation. Mueller and Seneviratne (2012) show that the dryness-temperature relationship is

440   important in many areas of the world including much of Eastern Europe (extending east into European

441   Russia to about 50°E), where the probability of occurrence of an above-average number of hot days

442   with preceding precipitation deficits is over 60%.   Volodin (2011) analyzed the causes of "super-

443   extreme" anomalies of summer surface air temperature in a suite of GCM experiments and reanalyses,

444   focusing on the summer 2010 hot spell over ER as well as similar hot spells in Western Europe (2003)

445   and the contiguous United States (in 1980 and 2007). He showed that, in addition to the atmospheric

446   factors acting during the peak month of drought (in the case of ER in July 2010 this was a prolonged

447   atmospheric blocking event), preceding monthly anomalies of soil moisture located windward of the

448   drought significantly enhanced the temperature anomaly. This behaviour repeated itself over ER in

449   the summer of 2012 where the drought (and the soil moisture anomaly) began initially over

450   Kazakhstan and the southernmost areas of ER and gradually expanded northward. Lorenz et al.

451   (2010) analyzed regional climate model simulations to show that soil moisture memory also acts to

452   increase the persistence (in addition to the intensity) of heat wave events.

453

454   Koster et al. (2006b, see their Figure 11) showed that the observed spatial pattern of interannual JJA

455   temperature variance over North America can be reproduced by an AGCM only when soil moisture

456   feedback processes are allowed to operate in the model, a strong indication that soil moisture

457   variability contributes significantly to temperature variability. An analogous figure for Eurasia is

458   shown here in Figure 5. Figure 5a, from observations (MERRA), shows monthly temperature

459   variance for the JJA period over 1980-2012. To first order, the free-running GEOS-5 AGCM (Figure

460   5b) reproduces this structure, with high variability in the most northern parts of Eurasia and another

461   band of high variability centered at about 50°N. (The variances produced by the free-running model

462   and MERRA differ mostly in their amplitudes, with weaker values seen in the former.) Figure 5c

463   shows the temperature variances generated by the GEOS-5 AGCM when soil moisture feedback

464   processes are artificially disabled, a condition achieved here by continually resetting the land model's

465   soil moisture prognostic variables to seasonally-varying climatological values (see Appendix A).

466   Disabling soil moisture feedback significantly reduces the variances along a swath through the center

467   of the continent, extending from southern Europe eastward across the Caucasus to Kazakhstan,

468   Mongolia, and northern China (Figure 5d). This swath of reduction is indeed where we expect it to

469   be, located at the transition between the wet climate to the north and the dry climate to the south;

470   evaporation variance associated with soil moisture variations tends to be maximized in such a

471   transition regime (see Koster et al. 2006b). In the AGCM, soil moisture feedback is unequivocally

472   responsible for enhanced temperature variance along this swath, and we can speculate that the same is

473   true in nature. We will come back to the role of the land later in our discussion of long-term trends

474   and predictability.

475

476   The role of SST in seasonal to decadal climate variability over Eurasia is also still not well

477   understood.   Again, much of the analysis of the role of SST has focused on impacts in Europe, though

478   a number of these studies have implications for regions to the east.   Ionita et al. (2012) analyzed the

479   self-calibrating Palmer drought index (van der Schrier et al. 2006) for the period 1901 – 2002 and

480   found considerable interannual and multi-decadal variability in summer moisture over Europe that

481   was tied to SST variability. In addition to a drying trend over Europe associated with warming SST

482   over all oceans, they found a link between previous winter La Niña and negative PDO events and

483   summer dry conditions over southern Europe extending into western Russia, with wet conditions over

484   the Scandinavian Peninsula, with the atmospheric anomalies resembling aspects of the PNA and (the

485   positive phase of the) NAO. They also found a link with the cold/negative phase of the AMO that

486   leads to summer drought conditions extending across southern Scandinavia, southeastern Europe and

487   into northwestern Russia. They cite the extremely hot and dry summers of 1921 and 1972 over the

488   central and northern regions of Russia (Buchinsky 1976) as examples of events that coincide with an

489   AMO in its negative phase.

490

491   Sedlacek et al. (2011) hypothesized that the SST anomalies in the Barents and the Arabian Seas

492   combined to produce warming over Eurasia during 2010, thus contributing to the heat wave; they

493   suggest that such a dynamic response to SST (in particular to the expected warming and reduction in

494   sea ice over the Barents Sea) will contribute to more frequent heatwaves over Eurasia in the future.

495   Wu et al. (2012) examined the impact of the North Atlantic Oscillation on the relationship between

496   the East Asian summer monsoon and ENSO and found, among other things, that an anomalous spring

497   NAO induces a tripole SST anomaly in the North Atlantic which persists into summer and excites

498   downstream development of a Rossby wave train that modulates the blocking highs over the Ural

499   Mountains and Okhotsk Sea. While the main impact of Arctic Sea ice reduction occurs during winter

500   (Deser et al. 2007), a recent observational study by Francis and Vavrus (2012) suggests that the

501   reduction in Arctic Sea ice slows the progression of Rossby waves by weakening the zonal winds and

502   increasing wave amplitude. They argue that while these impacts are strongest during winter and

503   autumn, they are also apparent in summer (possibly due to earlier snow melt on high-latitude land)

504   and therefore contribute to more extreme summer weather events including Eurasian heat waves.

505

506   *b. The role of Stationary Rossby waves*

507   A recurring theme in the above discussion is the role of Rossby waves. Ambrizzi et al (1995) provide

508   one of the first studies to isolate the teleconnectivity associated with the boreal summer wave-guides

509   and preferred wave propagation patterns towards and away from the wave-guides. Again, Schubert et

510   al. (2011) identified a particular recurring Rossby wave (forced by submonthly vorticity transients)

511   that extends across northern Eurasia and that contributes significantly to monthly surface temperature

512   and precipitation variability, playing an important role in the generation of the 2003 European and

513   2010 Russian heat waves.

514

515   To the extent that Rossby waves are an important component of summer Eurasian temperature and

516   precipitation variability, we would expect that the leading surface temperature and precipitation

517   REOFs shown in Figure 3 would be tied to such atmospheric waves. The correlations between the

518   leading RPCs and the monthly 250mb v-wind (Figure 6) suggest that this is indeed the case. The

519   correlations with the first two RPCs show two clear wave structures that are approximately in

520   quadrature extending across northern Eurasia. In fact these closely resemble the Schubert et al. (2011)

521   basic wave structure of the leading REOF of the monthly 250mb v-wind mentioned above. The

522   correlation pattern associated with the first RPC differs somewhat from that of the second in that the

523   anomalies seem to extend around the globe, and there is a clear signature of a split in the wave over

524   Europe with the northern component extending across Eurasia to the north of the mean jet, and a

525   southern component that appears to use the mean jet as a wave guide (this correlation pattern is very

526   similar to the actual 250mb v-wind anomalies during July 2010 – cf. Fig. 7). The correlations

527   associated with the second RPC suggest a wave development that is more confined to the northern

528   part of Eurasia (north of the mean jet), and resembles the June 2003 v-wind anomalies (Fig. 7).

529

530   The correlations with the third RPC (Figure 6) show a wave structure that is more confined to the

531   mean jet throughout the Northern Hemisphere; over Eurasia it appears to affect primarily southern

532   Europe and the regions east of the Caspian Sea. This pattern dominates the v-wind anomalies, for

533   example, in August 1992 (Fig. 7). The fourth and fifth RPCs are associated with wave structures

534   similar to those of the other leading modes, but with that of the fourth having its largest amplitude

535   over the eastern half of Eurasia (e.g., August 2001 in Fig. 7), and that of the fifth having its largest

536   amplitude over northeast Atlantic and northern Europe (e.g., July 1994 in Fig. 7).

537

538   The potential role of SST anomalies in forcing the leading REOFs was examined by computing the

539   simultaneous and time-lagged correlations with the global monthly SST anomalies (Figures not

540   shown). The results indicate that the correlations are generally weak (absolute values less than 0.3).

541   An exception to that is RPC1, which has somewhat larger negative correlations (between -0.3 and -

542   0.4) in the tropical eastern Pacific at both 0 and -1 month lags, suggesting a weak link to ENSO. Also,

543   RPC 3 has positive correlations with SST (between 0.3 and 0.4 at lag 0) over the North Atlantic, with

544   a similar pattern of correlations (but weaker) occurring at -1 lag. The largest correlations with SST

545   occur for RPC5 (values greater than 0.5 at lag 0) over the far eastern North Atlantic and

546   Mediterranean Sea in the immediate vicinity of Europe: these likely reflect the response of the SST to

547   the changes in atmospheric forcing associated with the wave itself. The above results indicate that

548   SSTs have only a weak (if any) impact on the development of these waves on monthly time scales,

549   with perhaps ENSO and the North Atlantic SST having some influence on RPCs 1 and 3, respectively.

550   An important caveat here is that the above correlations reflect primarily interannual linkages in the

551   monthly statistics, rather than subseasonal linkages. In fact, if we remove the interannual component

25

552   of the variability, the correlations with SST are even weaker for all RPCs except for the simultaneous

553   correlations associated with RPC 5 in the vicinity of Europe.

554

555   The forcing of such waves by submonthly vorticity transients is illustrated in Fig. 8 in the context of a

556   stationary wave model (SWM- Ting and Yu 1998) forced by an idealized localized vorticity source in

557   the North Atlantic jet exit region (see Schubert et al. 2011 for details). The results show that an

558   atmospheric wave structure very similar to that associated with REOF 1 develops in the SWM within

559   about three weeks. While such Rossby waves (driven by internal atmospheric dynamics) appear to be

560   a ubiquitous component of summertime weekly to monthly atmospheric variability over Eurasia, the

561   mechanism that leads to their occasional persistence and amplification are as yet unclear.   An

562   assessment of the potential role of soil moisture and a further assessment of SST forcing will be made

563   in the following two sections, where we examine longer-term (seasonal to decadal) variations and the

564   predictability of such extreme events.

565

566   **4. Past Long term Behavior and Trends**

567   *a) A Review*

568   The 2003 European and 2010 Russian heat waves, in addition to prompting numerous papers on

569   causes and impacts, highlighted the on-going debate about whether such events are early

570   manifestations of global warming. For example, Rahmstorf and Coumou (2011), employing a

571   stochastic model to examine the effect of warming trends on heat records, concluded that, with a

572   probability of 80%, "the 2010 July heat record would not have occurred" without the large-scale

573   climate warming seen since 1980, most of which has been attributed to the anthropogenic increase in

574   greenhouse gas concentrations. In contrast, as already mentioned, Dole et al. (2011) conclude from

575   their analysis of dynamical mechanisms that neither human influences nor slowly varying ocean

576   boundary conditions contributed substantially to the magnitude of the 2010 event.   Otto et al (2012)

577   examined the results from a large ensemble of atmospheric general circulation model simulations and

578   concluded that " there is no substantive contradiction between these two papers, in that the same event

579   can be both mostly internally-generated in terms of magnitude and mostly externally-driven in terms

580   of occurrence-probability. The difference in conclusion between these two papers illustrates the

581   importance of specifying precisely what question is being asked in addressing the issue of attribution

582   of individual weather events to external drivers of climate."

583

584   In addition to the current debate on whether the nature of extreme events is changing, there is also

585   ongoing debate about basic trends in both the mean precipitation and surface temperature.

586   Meshcherskaya and Blazhevich (1997) used station data to study changes in drought over the

587   European and Asian parts of the former Soviet Union (FSU) for the period 1891 – 1995. They found

588   that trends in their drought and excessive moisture index (DM, for May-July) are statistically

589   significant only in the Asian part of the FSU and that the increased dryness is largely the result of

590   temperature increases, with a small but statistically significant contribution coming from a decrease in

591   precipitation. These results have recently been updated and expanded by Groisman et al. (2013), who

592   showed that while heavy rainfall frequencies have increased in the past two decades, mean

593   precipitation has grown more slowly or has even decreased, with an accompanying increase in the

594   frequency of no-rain periods over most of Northern Eurasia south of 60°N.

595

596   Alexander et al (2006), using updated station data from the more recent record (1951-2003), examined

597   a number of climate indices (see also Frich et al. 2002) and found significant changes in extremes

598   associated with warming. In particular, they found that much of Eurasia is characterized by a

599   significant decrease in the annual number of cold nights and an increase in the number of warm

600   nights.   These results hold for all seasons, with the largest changes occurring during MAM and the

601   smallest during SON. Corresponding behavior is also seen in a subset of stations with records going

602   back to 1901. Precipitation indices show a tendency toward wetter conditions throughout the 20th

603   century.

604

605   Frey and Smith (2003) examined precipitation and temperature trends in station observations from

606   western Siberia, a region with a large percentage of the world's peatlands, and one that contributes

607   substantially to the terrestrial freshwater flux into the Arctic Sea. They found robust patterns of

608   springtime warming and wintertime precipitation increases, with the AO playing an important role in

609   non-summer warming trends. As noted by the IPCC (2001), the AO (and NAO) had been in phase

610   since the 1970s, producing enhanced westerlies and extratropical cold season warming across much of

611   Eurasia.

612

613   Batima et al. (2005) examined data from 60 meteo-stations spanning Mongolia for the period 1940-

614   2001 and found that the mean annual surface temperature has risen by 1.66°C over the 62-year period,

615   warming faster in winter than summer. The warming is more pronounced in mountainous areas and

616   their valleys and is less pronounced in the Gobi desert. They also find a statistically insignificant

617   decrease in annual mean precipitation, with winter and spring showing a decrease but summer and fall

618   showing no change. Even without clear evidence for an increase in summer temperatures, summer

619   heat wave duration has increased by 8-18 days, depending on location. 1998 was the warmest year of

620   the last century, and Mongolia experienced drought for the next four years (1999-2002). Batima et al.

621   (2005) further note that the intense drought spells in recent years are most likely the result of both

622   increased temperature and decreased precipitation. They emphasize that the environment and climate

623   plays a key role in the sustainability of Mongolia – animal husbandry employs 47.9% of the total

624   population, producing 34.6 percent of the agricultural gross production, and accounting for 30% of the

625   country's exports. Nandintsetseg et al. (2007) found an almost 2°C increase in temperature in

626   northern Mongolia between 1963-2002, along with a significant increase in warm extremes and a

627   decrease in cold extremes. On average, they found neither a significant decrease in the maximum

628   number of consecutive dry days nor an increase in the number of wet days

629

630   Robock et al. 2005 examined 45 years (1958-2002) of soil moisture observations over Ukraine and

631   found an increase in soil moisture over those years, despite a slight warming and a decrease in

632   precipitation. They suggested that this is the result of increased aerosols in the troposphere leading to

633   decreased solar insolation, which acts to reduce evaporation; the reduced evaporation in turn leads to

634   increased surface temperature and soil moisture.

635

636   IPCC (2007b, Table 10.2) summarize some of the key trends in northern Eurasia, with Russia

637   experiencing a 2 to 3°C rise in the past 90 years that is most pronounced in spring and winter.

638   Changes in precipitation in Russia are highly variable with a decrease during 1951 to 1995, and an

639   increase in the last decade. Central Asia experienced a 1-2 °C rise in temperature per century, with no

640   clear trend in precipitation between 1900 and 1996. Mongolia has seen a 1.8°C increase in the last 60

641   years that is most pronounced in winter; Mongolian precipitation has decreased by 7.5% in summer

642   and has increased by 9% in winter.

643

644   Analyses covering longer time periods are also available. Briffa et al. (1995) report on a 1000-year

645   tree-ring reconstruction of summer temperatures over the northern Urals; they show that the mean

646   temperature of the 20th century is higher than that of any other century since AD 914. Demezhko and

647   Golovanova (2007) reconstructed ground surface temperatures from AD 800 onward based on

648   borehole temperature logs and 170 years of meteorological data over the southern and eastern Urals.

649   They conclude that the mean temperature during the Medieval maximum (1100-1200AD) was 0.4°K

650   higher than that for the period 1900-1960. They also conclude that cooling during the "Little Ice Age"

651   culminated in about AD 1720 with a mean surface temperature 1.6°K below the 1900-1960 mean, and

652   they note that the contemporary warming began about a century prior to the first instrumental records

653   in the Urals, with the mean rate of warming increasing in the final decades of the 20th century.

654

655   The recent Special Report of IPCC on extremes (IPCC, 2012) provides an updated summary of the current

656   confidence placed in recent trends of heat waves and droughts. The report notes that in Asia there is "overall

657   low confidence in trends in dryness both at the continental and regional scale, mostly due to spatially varying

658   trends, except in East Asia where a range of studies, based on different indices, show increasing dryness in

659   the second half of the 20th century, leading to medium confidence."   They also note that since 1950, there is

660   medium confidence in a warming trend in daily temperature extremes over much of Asia.

661

662   *b) A model-based analysis of recent trends (1979-2012)*

663   In this section, we utilize numerical simulations to provide further insight into the nature of recent

664   variability and trends over Eurasia. These simulations take the form of full global reanalyses

665   (MERRA and ERA Interim), AMIP-style simulations using the GMAO GEOS-5 system, and

666   simulations with more idealized SST forcing.

667

668   One of the intriguing aspects of RPC 1 in Fig. 4 is the apparent trend or shift in the time series from

669   being predominantly negative prior to about 1995 to predominantly positive thereafter. There is an

670   indication of a similar shift in RPCs 3 and 4. The first three panels on the left of Fig. 9 (derived from

671   the two reanalyses and from station observations) indicate that these shifts appear to be part of a

672   hemispheric-wide pattern of warming over the last three decades, with the maxima over Eurasia

673   centered over European Russia and Mongolia/eastern Siberia. While the maps from the reanalyses

674   differ somewhat from that constructed with the station observations, especially regarding the

675   amplitude of the changes, overall they agree on the main regions of warming. As for precipitation

676   (the first three panels on the right side of Fig. 9), the patterns of change are more complex, with

677   decreases covering parts of northeastern Europe, European Russia, Kazakhstan, southeastern Siberia,

678   Mongolia, and northern China, and with increases found across Siberia north of about 60°N.

679

680   The extent to which the above trends are a reflection of global warming and/or the result of other

681   long-term (decadal) variability is still an open question. Some insight into this issue can be gained

682   from the analysis of free-running climate model simulations. We examine now an ensemble of 12

683   GEOS-5 AMIP simulations driven by observed SST and GHG forcing over the period 1871-present.

684   The 1996-2011 minus 1980-1995 differences for the ensemble mean are shown in the bottom panels

685   of Figure 9. Overall the model results are consistent with the reanalyses and observations, showing

686   warming over basically the same regions across Eurasia (southern Europe and European Russia,

687   Kazakhstan/southern Siberia, Mongolia, and northern China) though with weaker amplitude. We

688   note, however, that individual ensemble members (not shown) exhibit changes as large as the

689   observed and that there is substantial intra-ensemble variability in the detailed spatial patterns of the

690 differences, with some showing the same two-lobed structure found in the observations. The model

691 ensemble mean also reproduces to some degree the overall pattern of precipitation changes (though

692 again with weaker amplitude than observed), including the tendency for precipitation deficits over

693 European Russia and over Siberia south of about 60°N, and for precipitation increases to the north.

694

695 The AMIP results in Figure 9 suggest that SST variations and perhaps the direct GHG forcing are

696 contributing significantly to the observed JJA trends in Eurasian surface temperature and precipitation

697 seen over the last three decades. Figure 10 (left panel) shows the linear trend in observed SST during

698 that period (1980-2011). The SST trend pattern shows aspects of overall warming combined with a

699 La Niña-like pattern in the Pacific and a positive Atlantic Multi-decadal Oscillation (AMO) pattern in

700 the Atlantic. This is compared (right panel of Fig. 10) with one of the idealized SST forcing patterns

701 used recently by the USCLIVAR Drought Working group to force several different climate models

702 (Schubert et al. 2009). This latter pattern is the sum of the three leading REOFs of annual mean SST,

703 consisting of a PDO/La Niña -like pattern, an AMO-like pattern and the warming trend pattern. With

704 the exception of the Indian Ocean, the similarity of this idealized pattern to the recent (three decade

705 long) trend pattern is striking, suggesting that the recent trends are a mixture of both decadal

706 variability and long-term trends.

707

708 Figure 11 shows, for the average of three of the models that participated in the USCLIVAR Drought

709 Working group project (Schubert et al., 2009) and GEOS-5, the JJA surface temperature response to the

710 idealized SST pattern shown in the right panel of Fig.10. The results are based on 50-year long simulations

711 for all the models except CFS which was integrated for 35-years. The models produce warming (top left

712 panel) over most of Eurasia between 30-60°N. The precipitation anomalies (top right) consist of deficits

713   over central Eurasia (centered on about 50°N, 95°E) and parts of Europe. Positive precipitation anomalies

714   occur over much of the northern regions of Russia, especially east of about 70°E, extending into northeastern

715   China. Additional runs with these models (not shown) indicate that the Pacific and Atlantic SST patterns act

716   to focus the warming and precipitation deficits in the middle latitude band between 30-60°N, as well as to

717   produce some regional (east/west) variations that differ from model to model. The SST trend pattern acts to

718   expand and enhance the regions of warming, with an overall tendency to warm the continents everywhere.[9]

719   These results are generally consistent with those shown in Fig. 9, supporting the idea that the main features

720   of the northern Eurasian precipitation and temperature trends of the last three decades are largely forced by

721   the leading patterns of SST variability (the global trend and the two dominant patterns of SST variability in

722   the Pacific and Atlantic Oceans). The bottom panel of Figure 11 suggests that the surface warming and

723   precipitation changes are linked to a tendency for all the models to produce a band of positive upper

724   tropospheric height anomalies throughout the middle latitudes of both hemispheres in response to the

725   imposed SST patterns, and that (as shown by additional runs isolating the SST trend impacts – not shown)

726   these positive height anomalies, while basically forced by the Pacific and Atlantic SST patterns, are

727   amplified with the additional forcing of the SST trend pattern.

728

729   *c) An Analysis of Long-Term Variability (1871-2010)*

730   To put the trends of the last three decades in perspective, we now turn to temperature records going

731   back to the late 19th century. The left panels in Figure 12 show the time series of JJA mean

732   temperature for the period 1871 to 2010, based on the CRUTEM4 data, for four different regions in

733   northern Eurasia: Europe, European Russia, south-central Siberia, and a cold desert region just east of

734   the Caspian Sea, centered on the Aral Sea. (The definition of the regions was guided by the regions of

_____

[9] There are some regions of cooling over land in response to the SST trend pattern (which itself has some spatial variability)
though these tend to be relatively small in area and have small amplitude of cooling.

735 maximum T2m loadings of the leading REOFs shown in Fig. 3.) All four regions show

736 predominantly positive anomalies beginning shortly after 1990, though this is most pronounced for the

737 European region. The 2010 heat wave stands out in the European Russia time series, though there are

738 some other years with large anomalies, including 1972 (during the "100-year" drought; see also

739 Appendix B). While there is substantial interannual and decadal scale variability in all of the time

740 series, there is also evidence of a long-term positive trend, though the trend values appear to depend

741 somewhat on the observations during the late 19th century, which are likely not very reliable in the

742 CRUTEM4 data set. This is illustrated through comparison with another data set (NOAA MLOST –

743 right panels of Fig. 12), indicating some differences during the early years, especially for the more

744 eastern region. The latter dataset shows clearer long-term trends in part because it does not include

745 the 1870s, which in the CRUTEM4 data is a period of positive anomalies. Note that extensive

746 *standard* surface air temperature observations over the Russian Empire territory began in 1881

747 (Vannari 1911).

748

749 Figure 13 is the same as Figure 12, but constructed from the output of two representative members of

750 the aforementioned 12-member ensemble of 130-yr AMIP simulations with GEOS-5 (see Appendix

751 A). Each time series shows a basic character that is remarkably similar to that of the observations,

752 with a shift towards positive anomalies starting in the 1990s. The long-term trend in all four regions

753 is, in fact, even more pronounced in the model simulations. The simulations also show a few very

754 extreme anomalies. In particular, we point out the unusually large positive (+3°C) anomaly simulated

755 in 2001 in European Russia in one of the ensemble members (second row of Fig. 13, on left). This

756 event has a temperature signal comparable in magnitude to that observed during the 2010 Russian heat

757 wave (Fig. 12) and will be examined in more detail in the next section. We note that similar events

758 (temperature anomalies near +3°C) occur in some of the other ensemble members, though in general

759 they are quite rare and are limited to the recent decades (e.g., there were only three such events in

760 Europe and only two in European Russia in the entire ensemble of 12 runs, i.e., over a span of 1680

761 simulation years).

762

763 We next examine whether the interannual JJA mean surface temperature (T_s) variations in these

764 regions are linked to SST variability. Figure 14 shows the temporal correlations of the regional mean

765 T_s for the European Russia region with T_s values everywhere across the globe (using SST over the

766 oceans). The calculation is limited to the years 1901-1980 in order to avoid the earliest years with

767 little observational data and to avoid the three most recent decades, which show the shift towards

768 positive values. In addition, a linear trend was removed from all time series prior to computing the

769 correlations.   The results for the observations (top panel)[10] show a wave structure over northern

770 Eurasia that is very similar to the leading REOF of the monthly data for the recent three decades (Fig.

771 3 top left panel), suggesting that the seasonal data also project onto a Rossby wave structure,

772 consistent with the findings of Schubert et al. (2011). There are also positive correlations over the

773 Atlantic and the eastern Pacific, suggesting some link to the SST. The results for the model are shown

774 in the middle and bottom panels of Figure 14. The middle panel shows the correlations computed

775 separately for each ensemble member and then averaged over the 12 ensemble members – a result that

776 is more comparable to the correlations based on the observations. The model results clearly show the

777 same basic wave structure of the correlations over northern Eurasia. By this measure, the link to the

778 oceans is weak, with only small positive correlations (0.1-0.2) that are mainly confined to the Atlantic,

779 however, there are individual ensemble members (not shown) that have correlations resembling those

780 based on the observations (highlighting a considerable unforced component to the observational

---

[10] Absolute values greater than 0.22 are significant at the 0.05% level (*www.mtsu.edu/~dwalsh/436/CORRSIG.pdf*)

781 results). The bottom panel in Figure 14 shows the correlations with the ensemble mean T_s. This

782 calculation isolates the impact of the forcing common to all the ensemble members (SST and GHGs),

783 showing, for example, correlations over the North Atlantic that exceed 0.4.   Also, it is noteworthy

784 that the pattern of correlations over the eastern Pacific is very similar to that based on the

785 observations.   Other regions with relatively large correlations include Northern Africa, southern

786 Eurasia, Canada and the western US. Further analysis (not shown) indicates that the patterns of the

787 correlations are quite sensitive to the location of the target area. Analogous global maps of T_s

788 correlations with T_s values in southern Europe, for example, show substantial negative correlations in

789 the tropical Pacific and the Indian Ocean (for the ensemble mean), as well as positive correlations

790 with the North Atlantic SST; the spatial pattern of these correlations over the ocean indeed resembles

791 the spatial pattern of the SST anomalies shown in Fig. 10.

792

793 In summary, there appear to be significant temporal correlations between JJA surface temperature

794 over large regions of Eurasia and SST, particularly in the North Atlantic and the tropical Pacific.

795 However, the SST-forced response appears to be intertwined with and sensitive to the excitation of the

796 basic internally-generated Rossby wave structures discussed previously. This aspect of the response is

797 currently not well understood.

798

799

800 **5. Predictability and Projections**

801 In this section we review and provide new results on the predictability of drought and heat waves. We

802 also review studies that examine longer-term projections, including those that examine overall trends

803 in precipitation and temperature and provide an outlook for future heat waves and droughts.

804

a) A Review of Predictability

806 The predictability of heat waves and associated droughts is particularly challenging in view of their

807 strong link to the development of persistent anticyclones, blocking, and stationary Rossby waves (see

808 previous section on mechanisms). Most weather and climate models do not adequately represent

809 blocking events (e.g., Scaife et al. 2010); they underestimate the occurrence of blocking as well as its

810 intensity and duration.   In addition, the basic predictability of blocking is likely rather short (perhaps

811 a few weeks), since blocking ridges are believed to be maintained by interactions with smaller scale

812 weather systems (e.g., Scaife et al. 2010). The aforementioned results tying the development of major

813 Eurasian heat waves to stationary Rossby waves also indicates relatively short predictability time

814 scales, since the main forcing of such waves appears to be sub-monthly weather transients (e.g.,

815 Schubert et. al. 2011). We note that the link between Rossby waves and the development of blocking

816 events is still unclear (e.g., Nascimento and Ambrizzi 2002; Woollings et al. 2008).

817

818 Soil moisture anomalies and associated land-atmosphere feedbacks do provide some hope for skillful

819 predictions out to perhaps 2 months (i.e., beyond weather time scales), though the levels of attainable

820 skill, particularly given the observational networks available for soil moisture initialization, are

821 modest at best (Koster et al. 2012; see also Volodin 2011). As discussed above, it is still an open

822 question whether links to SST variability are sufficiently robust to provide useful forecast skill at

823 seasonal to interannual time scales, though there is some evidence that Arctic sea ice changes could

824 provide some predictable signals. Modes of variability such as the NAO, the NAM, East

825 Atlantic/Western Russia (EA/WR) and the Scandinavian modes, while primarily associated with cold

826 season variability, can also play a role by preconditioning the soil moisture for the subsequent

827   summer. While the NAO appears to have limited predictability on monthly and longer time scales

828   (e.g., Johansson 2007), being largely driven by internal atmospheric dynamics, some evidence

829   suggests that predictability may be provided through the coupling of the NAM with the stratosphere

830   (e.g., Körnich 2010). Basic understanding of the mechanisms and predictability of the EA/WR and

831   Scandinavian modes is not well understood. Monsoonal flows (e.g., Trenberth and Fasullo 2012)

832   provide another potential source of predictability, though the current capability of simulating Asian

833   monsoon variability is quite limited.

834

835   The 2010 heat wave provides an important example of our current ability to predict a particularly

836   extreme event. Matsueda (2011), using medium range ensemble forecasts, showed some success in

837   predicting aspects of the blocking and extreme surface temperatures associated with the event out to a

838   lead time of 9 days, though the later stages of the blocking in early August were less well predicted,

839   with most models predicting a too early decay of the blocking. Ghelli et al. (2011) found signs of the

840   developing heat wave about 3 weeks in advance in predictions with the ECMWF's suite of models,

841   though the full amplitude of the event was not predicted until about 1 week in advance.   These results

842   are consistent with the study by Dole et al. (2011), which found no change in the probability of

843   prolonged blocking events over western Russia during July 2010 for forecasts initialized in early June

844   of that year, compared with hindcasts initialized in early June of other years (1981-2008).

845

846   *b) A Case Study*

847   Here, using a more idealized approach, we present new results concerning the basic predictability of

848   extreme heat waves and associated drought events. We examine the predictability of one of the most

849   extreme events to occur over European Russia in our multi-decadal GEOS-5 AMIP simulations: the

850   extreme heat event simulated by one of our ensemble members in the summer of 2001 (see discussion

851   of Fig. 13). We remind the reader that the fact that this event happened to occur in 2001 in the

852   simulation (rather than 2010 as in nature) appears to be purely by chance, since there is no consistency

853   among the various ensemble members as to the timing of such events.   Here we chose the event that

854   occurred in 2001 in ensemble member 6 because it was one of the most extreme simulated events to

855   occur over basically the same region as the observed event of 2010. Figure 15 shows the evolution of

856   the surface air temperature, upper tropospheric meridional wind, and soil moisture from May through

857   August of that year. The surface air temperature anomalies during May show a wave structure across

858   northern Eurasia, the same structure that characterizes the monthly variability of observations (e.g.,

859   Fig. 3).   At this time the largest temperature anomalies occur over eastern Siberia, with negative

860   anomalies to the west and positive anomalies over Eastern Europe and European Russia. The same

861   basic structure continues into June, showing some propagation to the east and intensification of the

862   warm anomalies over European Russia, especially just north of the Black Sea, where it achieves its

863   maximum amplitude of more than 5°C. By July the wave structure is more diffuse, but the warm

864   anomalies over European Russia continue through July and well into August. The upper level wind

865   shows that the Ts anomalies are associated with Rossby wave-like structures that develop in May,

866   peak in June, and dissipate thereafter.   The soil moisture anomalies show the same basic wave

867   structure, though somewhat phase shifted to the east of the temperature anomalies. The negative soil

868   moisture anomalies over European Russia are already evident in May (just north of the Black and

869   Caspian Seas), intensifying in June and continuing through July into August. As the Ts anomalies

870   move to the east, they appear to become phase locked with the soil moisture anomalies beginning with

871   July and extending into August.

872

873   Our interpretation of the above results is that the heat wave was initiated by the development of a

874   Rossby wave (May and June). This wave generated Ts anomalies that eventually became phase

875   locked with existing dry soil moisture anomalies over European Russia, which acted to intensify and

876   persist the Ts anomalies beyond the lifespan of the Rossby wave. We note that central ER

877   (specifically the region 30°E-48°E, 50°N-60°N) in that ensemble member experienced soil moisture

878   deficits for almost a decade from the mid 1990s to early 2003, deficits that appear to be part of a

879   general drying and warming trend (evident also in the ensemble mean) that begins in the mid-20th

880   century and becomes especially pronounced after the mid-1990s. This suggests that the SST/GHG

881   forcing may have set the stage for the development of the extremely warm summer over European

882   Russia.   We note that the evolution described here is quite similar to that found in Lyon and Dole

883   (1995) for the 1980 and 1988 U.S. drought cases, where anomalous wavetrains associated with early

884   stages of heat wave/droughts became very weak by early July, with reductions in evapotranspiration

885   over the drought regions intensifying and prolonging the excessive heat into later summer. It remains

886   to be seen whether GHGs may have set the stage for the development in these observed cases or

887   whether naturally occurring drought would lead to the same outcome,

888

889   We investigate the predictability of this event by performing a supplemental set of 20 simulations,

890   each initialized on 0z, 15 May 2001 and run through August. Each simulation differs from the control

891   (i.e., the ensemble member that produced the extreme event in Figure 15) only in the initialization of

892   the atmosphere; to produce the atmospheric initial conditions, a small perturbation was added to the

893   control atmosphere's state on May 15. The results are presented in Figure 16. The left column shows

894   the Ts anomalies from the control simulation, the middle column shows those for the ensemble mean

895   of the perturbation experiments, and the right column shows the ensemble mean of the soil moisture

896   anomalies. In the ensemble mean, the wave structure in Ts is largely gone by June, indicating that in

897   the span of a few weeks, the Rossby wave producing it has already lost all predictability. What

898   remains in June is a general warm anomaly along the [40°N,50°N] latitudinal belt of continental

899   Eurasia. This warming lasts into July and August over southern European Russia (the core of the

900   original Ts anomaly) and is collocated with the dry soil wetness anomalies, suggesting that the land

901   anomalies act to maintain the Ts anomalies several months beyond the predictability limit of the

902   Rossby wave.

903

904   In summary, for at least some extreme heat wave and drought events, predictability associated with

905   stationary Rossby waves, which are largely forced by submonthly transients, appears to be limited to

906   perhaps 2-3 weeks. Nevertheless, there appears to be some longer-term predictability tied to the

907   persistence of soil moisture anomalies. Ties to SST variations could provide some predictability on

908   seasonal and longer time scales, though SST impacts appear to be intertwined with the underlying

909   internally forced and shorter-time scale Rossby wave structures, and this connection is currently

910   poorly understood.

911

912   *c. A Review of projections for the future*

913   We now address the question of how heat waves and droughts might manifest themselves in a future,

914   warmer world.

915

916   Galos et al. (2007) reviewed drought occurrence in Hungary, noting that annual mean temperatures

917   became warmer in the second half of the 20th century, accompanied by a significant increase in

918   drought frequency. In particular, summers for the period 1990-2004 were warmer than those of the

919   previous 30 years. The period 1983-1994 was an extraordinarily dry period, with severe droughts in

920   the Carpathian Basin of Hungary. They found from an analysis of REMO 21st Century simulations (a

921   limited area model forced by lateral boundary conditions from three different ECHAM5/MPI-OM

922   GCM runs - IPCC scenarios B1, A1B, and A2) that the probability of dry summers will not increase in

923   the first half of the 21th Century, but the intensity of dry events will increase due to the higher

924   temperatures. They also found, however, that during the second half of the 21st century both the

925   number and intensity of dry events will increase significantly.

926

927   Meehl and Tebaldi (2004) examined simulations of 20th and 21st Century climate produced by the

928   global Parallel Climate Model (PCM), which used a "business as usual" emission scenario for the 21st

929   Century. They found the circulation patterns associated with heat waves in North America and

930   Europe to be intensified in the 21st Century, implying that future heat waves will be more intense,

931   more frequent, and longer lasting in the second half of that century.

932

933   Barriopedro et al. (2011) show that the 2003 and 2010 summer heat waves likely produced the

934   warmest seasonal temperatures seen in 500 years over about 50% of Europe. They conclude, based on

935   regional climate model simulations driven by different GCMs forced by A1B emission scenarios, that

936   the probability of a summer mega-heat wave over Europe will increase by a factor of 5 to 10 in the

937   next 40 years, though the probability of an event with the magnitude seen in 2010 will remain

938   relatively low until the second half of the 21st century.

939

940   The Special Report of IPCC on extremes (IPCC, 2012) gives drought projections low confidence due

941   insufficient agreement among the individual projections resulting from both model differences and

942   dependencies on the definition of drought (e.g., soil moisture versus precipitation-based indices). On the

943   other hand, they conclude that is very likely that the length, frequency, and/or intensity of heat waves

944   (defined with respect to present regional climate) will increase over most land areas. In particular over the

945   high latitudes of the Northern Hemisphere, a 1-in-20 year annual hottest day is likely to become a 1-in-5 year

946   annual extreme by the end of the 21st century, under the SRES A2 and A1B emission scenarios.

947

948

949   **6. Summary and Concluding Remarks**

950   Drought and heat waves often go hand in hand. While this can of course simply be because drier soils

951   produce less evaporative cooling of the surface, in northern Eurasia persistent anticyclones appear to play a

952   key role, acting to both warm and dry the atmosphere and land surface over many important agricultural

953   regions, from European Russia to Kazakhstan and beyond.   The importance of anticyclones in the

954   development of droughts was known as far back as the early 20th Century (e.g., Buchinsky 1976; also the

955   review of earlier literature in Obukhov et al. 1984). Different air masses are linked to the development of

956   anticyclones, especially the intrusion of Arctic air masses that occasionally combine with subtropical air

957   (e.g., associated with the Azores high in eastern Europe and western Russia); a basic understanding for how

958   these air masses produce especially severe droughts across Eurasia was already established by that time (e.g.,

959   see summary by Kleshenko et al. 2005).   Perhaps less well understood, though mentioned in early historical

960   documents, was the tendency for especially severe droughts and heat waves to be juxtaposed with wet and

961   cool conditions in regions thousands of miles to the east or west (see Section 1).   Observational studies also

962   established that while droughts across northern Eurasia rarely last for more than 2 months (Cherenkova,

963   2008), there is considerable evidence for longer (even multi-year) droughts to occur in the more southern

964   marginal semi-arid and arid regions of northern Eurasia (e.g. in Kazakhstan during the 1930s: cf., Kahan

965   1989; Almaty 2006, or over the Great Steppe of Central and East Asia: cf., Gumilev 1960).

966

967   Here we provide an updated picture of the role of anticyclones in northern Eurasian summer climate

968   through an analysis of the last three decades of monthly surface temperature and precipitation

969   variability and covariability, using the latest generation of reanalyses and gridded station observations.

970   We also examine longer-term changes (including the recent decadal changes) in surface temperature

971   and precipitation over Eurasia and the interannual variability of these quantities over the last century

972   or so, using model simulations (especially those with the GEOS-5 AGCM) to better understand the

973   nature of the variability.

974

975   Among the key new results of this study is the quantification of the major summer patterns of monthly

976   surface temperature and precipitation variability across northern Eurasia and the link between these

977   patterns and stationary Rossby waves. The characteristic east-west wave structure of the leading

978   patterns of surface meteorological variables are a reflection of these waves which, when amplified and

979   stationary, appear to have led to some of the most extreme heat waves and droughts in Eurasia (e.g.,

980   the 2003 European and 2010 Russian heat waves), with anomalies of opposite sign occurring to the

981   east and/or west depending on the phase and location of the wave. These waves appear to be initially

982   forced upstream of Eurasia (e.g., within the North Atlantic jet exit region [Schubert et al. 2011]); the

983   wave energy propagates over northern Eurasia, north of the mean jet and/or further to the south where

984   it remains confined to the mean jet. The structure of these waves and their time scales (weeks to a

985   few months) are consistent with past observations of the structure and time scales of heat waves and

986   droughts across northern Eurasia.

987

988 The GEOS-5 AGCM simulations forced with observed SSTs and GHGs show heat waves that appear

989 to be linked to Rossby waves occurring over Eurasia, including some rare, very extreme events during

990 the last few decades. A case study of one of the most extreme heat waves to occur in the model

991 (during the "summer of 2001" of one ensemble member) shows that the associated Rossby-like wave

992 pattern in the surface temperature anomalies is for the most part unpredictable beyond about 1 month.

993 Some aspects of the heat wave are, however, predictable for several months: these are the surface

994 temperature anomalies at the center of the heat wave associated with soil moisture anomalies that

995 persist through the summer. An inspection of the precursors to the heat wave show existing dry soil

996 moisture anomalies (especially pronounced in that ensemble member) that are part of a long term

997 drying and warming trend simulated in the model, a trend that is consistent with observations. More

998 generally, the impact of land-atmosphere feedbacks was quantified with model simulations in which

999 the soil moisture feedbacks were disabled. These runs show that temperature variability is especially

1000 strongly tied to soil moisture variability in the southern parts of our study area extending from

1001 southern Europe eastward across the Caucasus, Kazakhstan, Mongolia, and northern China.

1002

1003 Our investigation of the warming that has been observed over northern Eurasia in the last three

1004 decades shows that it is part of a large-scale pattern of warming with local maxima over European

1005 Russia and over Mongolia/eastern Siberia. Precipitation changes consist of deficits across Eurasia

1006 covering parts of northeastern Europe, European Russia, Kazakhstan, southeastern Siberia, Mongolia,

1007 and northern China. Precipitation increases occur across Siberia north of about 60°N. Remarkably,

1008 the ensemble mean of the AGCM simulations forced with observed SST and GHGs to a large extent

1009 reproduces the observed surface temperature and precipitation trend patterns of the last three decades,

1010   though with smaller amplitude. This suggests that some of the basic features of the observed trends

1011   over Eurasia are associated with an SST trend that consists of a PDO-like colder Pacific and an AMO-

1012   like warmer Atlantic. Various model simulations (Schubert et al. 2009) carried out with idealized

1013   versions of these basic SST patterns indicate a global scale response to the PDO-like and AMO-like

1014   patterns, a response that is intensified by a global warming SST trend pattern. The dynamical

1015   response of the models to the SST forcing consists of a zonally symmetric positive upper tropospheric

1016   height anomaly in the middle latitudes of both hemispheres that appears to provide the large-scale

1017   atmospheric teleconnections linking the various regions of the world. We speculate that such a

1018   response was responsible for the synchronicity of droughts in such disparate regions as the Eurasian

1019   grainbelt (spanning Russia, Ukraine, and Kazakhstan) and the US Great Plains during, for example,

1020   the 1930s, as well as the drought and extreme heat in the same regions during the summer of 2012. It

1021   is also suggested that the longer time scales of dry conditions in the more southern regions of northern

1022   Eurasia may be induced by global SST anomalies.

1023

1024   A survey of the literature indicates a general consensus that the future holds an enhanced probability

1025   of heat waves across northern Eurasia especially by the second half of the 21st Century, while there is

1026   less certainty regarding future drought, reflecting the greater uncertainty in precipitation and soil

1027   moisture projections compared with temperature.   It is also clear that there are still gaps in our

1028   understanding of the physical mechanisms that control the intensity, duration and frequency of heat

1029   waves and droughts.   Perhaps most important are the uncertainties that remain in our understanding

1030   of the interactions between the short-term atmospheric variability associated with extremes, and the

1031   longer-term variability and trends associated with soil moisture feedbacks, SST anomalies, and an

1032   overall warming world.

1033

1044

1045   **Appendix A**: Observational Datasets and Model Simulations

1046   *A1. Observations and Reanalyses*

1047   Our analysis is based in part on MERRA (Rienecker et al. 2011). MERRA is an atmospheric reanalysis that

1048   was produced with the Goddard Earth Observing System Data Assimilation System Version 5 (GEOS-5)

1049   documented in Rienecker et al. (2008), consisting of the GEOS-5 atmospheric model and the Grid-point

1050   Statistical Interpolation (GSI) analysis system, the latter being a system jointly developed by the GMAO and

1051   NOAA's National Centers for Environmental Prediction. The GEOS-5 assimilation system includes an

1052   incremental analysis update (IAU) procedure (Bloom et al. 1996) that slowly adjusts the model states toward

1053   the observed state. This has the benefit of minimizing any unrealistic spin down (or spin-up) of the water

1054   cycle. MERRA was run at a resolution of ½° latitude × 2/3° longitude with 72-levels extending to 0.01hPa.

1055   More information about MERRA can be found at: http://gmao.gsfc.nasa.gov/research/merra/. The MERRA

1056   data used in this study (Ts, T2m, Precip, V250) were all taken at the full resolution of ½° latitude × 2/3°

1057   longitude covering the period 1979-2010.   Limited comparisons are made with ECMWF's ERA-interim

1058   reanalysis (Dee et al. 2011a,b).

1059

1060   We also make use of various station observations. These are the NOAA NCEP CPC GHCN_CAMS

1061   gridded two-meter temperature (Fan et al. 2008) - a 0.5°X0.5° degree latitude/longitude resolution

1062   dataset covering the period January 1948-January 2013.   We also make use of the CRUTEM4 two

1063   meter temperature station data gridded to 5° X 5° latitude/longitude for the period 1850-2012 (Jones et

1064   al. 2012), and the NOAA Merged Land-Ocean Surface Temperature Analysis (MLOST, Voss et al.

1065   2012), V3.5.2 also at 5° X 5° latitude/longitude for the period 1880-present. For the precipitation

1066   data, we use NOAA's precipitation reconstruction over land (PRECL) on a 1° latitude/longitude grid

1067   for the period 1948-2013 (Chen et al. 2002). The other precipitation data used in the study is version

1068   2.2 of the combined Global Precipitation Climatology Project (GPCP) data available on a 2.5° X 2.5°

1069   grid from 1979 to June 2011 (Adler et al. 2003).

1070

1071   *A2. The GEOS-5 Model and Simulations*

1072   We take advantage of an ensemble of 12 AMIP-style simulations carried out with the NASA Goddard

1073   Earth Observing System (GEOS-5) Atmospheric General Circulation Model or AGCM (Rienecker et

1074   al., 2008) forced with observed SST for the period 1870 -2012. The runs were started from different

1075   atmospheric and land initial conditions. Ten of the twelve ensemble members were run with

1076   interactive aerosols, while the other two used a prescribed aerosol climatology. We have found no

1077   discernable difference in the basic climatology and time dependence due to the treatment of the

1078   aerosols, so for the purposes of this study our ensemble means are based on all twelve runs. We also

1079   present some results on the impact of soil moisture feedback (Section 3a). Those results are based on

1080   two thirty-three year simulations for 1980-2012 forced with observed SST[11]. The first was run with

1081   interactive land, while the second was run with specified climatological soil moisture computed as an

1082   average of a previously run multi-decadal simulation. Details of the model are described next.

1083

1084   The GEOS-5 AGCM employs the finite-volume dynamics of Lin (2004). This dynamical core is

1085   integrated with various physics packages (Bacmeister et al., 2006) under the Earth System

1086   Modeling Framework (Collins et al., 2005) including the Catchment Land Surface Model (Koster

1087   et al., 2000), and a modified form of the Relaxed Arakawa-Schubert convection scheme described

1088   by Moorthi and Suarez (1992). For the experiments described here we used version 2.4 of the

---

[11] In practice these two runs were reinitialized November 1 of each year from a previous long model simulation forced with observed SST.

1089 AGCM. The model was run with 72 hybrid-sigma vertical levels extending to 0.01hPa, and 1°

1090 (about 100km) horizontal resolution on a latitude/longitude grid.

1091

1092 The CO_2 consists of the time varying annual global mean values provided by IPCC/CMIP5. The

1093 other greenhouse gases (GHGs: CH_4, N_2O, CFC-11, CFC-12, and HCFC-22), stratospheric water

1094 vapor (H_2O), and ozone (O_3) are relaxed to time varying zonal averages with a two-day e-folding

1095 time. The zonal averages of the GHGs are taken from simulations of 1950-2010 with the GEOS

1096 chemistry climate model (CCM, Pawson et al., 2008), and are calibrated (bias corrected) to the

1097 tropospheric concentrations specified by CMIP5 (Meinshausen et al., 2011). Stratospheric H_2O is

1098 also taken from the CCM. In both cases, GHGs and H_2O, five-year running averages are first

1099 computed to reduce the influence of interannual variability in the CCM fields. Ozone is specified

1100 from AC&C/SPARC monthly averages (ftp-esg.ucllnl.org) from 1870-2005, and is converted to

1101 zonal means before interpolation onto GEOS-5 layers. For all seven gases, the relaxation fields

1102 have realistic latitudinal, vertical, and seasonal variations imposed on their specified trends. Two-

1103 day e-folding times allow the species contours to sufficiently follow planetary-scale potential

1104 vorticity deformations in the stratosphere.

1105

1106 Aerosols are computed using the Goddard Chemistry, Aerosol, Radiation, and Transport model

1107 (GOCART, Chin et al. 2002; Colarco et al. 2009) in GEOS-5. The GOCART module is run

1108 online within the GEOS-5 AGCM; that is, the aerosols and other tracers are radiatively interactive

1109 and transported consistently with the underlying hydrodynamics and physical parameterizations

1110 (e.g., moist convection and turbulent mixing) of the model. GOCART treats the sources, sinks,

1111 and chemistry of dust, sulfate, sea salt, and black and organic carbon aerosols. Aerosol species are

1112   assumed to be external mixtures. Total mass of sulfate and hydrophobic and hydrophilic modes of

1113   carbonaceous aerosols are tracked, while for dust and sea salt the particle size distribution is

1114   explicitly resolved across 5 non-interacting size bins for each.

1115

1116   Both dust and sea salt formulations have wind-speed dependent emission functions, while sulfate

1117   and carbonaceous species have emissions principally from fossil fuel combustion, biomass

1118   burning, and biofuel consumption, with additional biogenic sources of organic carbon. Sulfate has

1119   additional chemical production from oxidation of SO_2 and DMS, and we include a database of

1120   volcanic SO_2 emissions and injection heights. For all aerosol species, optical properties are

1121   primarily from the commonly used OPAC data set (Hess et al. 1998). This framework also

1122   includes the representation of CO tracers, which have emissions from fossil fuel, biofuel, and

1123   biomass burning. The online CO processes in GEOS-5 derive from Bian et al. (2007), and include

1124   indirect production of CO from oxidation of natural and anthropogenic non-methane

1125   hydrocarbons, chemical production from methane (CH_4) oxidation, and losses through reaction

1126   with OH.

1127

1128   **Appendix B**: Northern Eurasian Droughts and Heat Waves since 1875.

1129   Here we briefly review some of the key metrics that have been used to characterize drought and heat

1130   waves over Northern Eurasia. We also include some further information (in addition to that already

1131   provided in the text) on past droughts and heat waves over this region. Table B1 is a compilation of

1132   the droughts and heat waves that have occurred since 1875, based on various scientific publications as

1133   well as the popular literature (references are noted in the table). The table also includes information

1134   on the regions affected, and other auxiliary information (comments) of potential use to those

1135   interested in investigating these events further. Years in bold indicate major droughts or heat waves,

1136   though it must be kept in mind that these are very subjective assessments of the relative severity of the

1137   various events, since they are based on differing metrics that emphasize varying aspects of

1138   meteorological, agricultural and hydrological droughts (and heat waves), over different time periods.

1139   As such, Table B1 should be considered as a convenient starting point for further investigation of the

1140   various droughts and heat waves that have occurred over Northern Eurasia in the last 135 years or so,

1141   rather than an objective comparative assessment of all droughts and heat waves that have occurred

1142   over this very large region. In fact we view this table (in the spirit of the GDIS effort mention earlier)

1143   as the starting point for a continually evolving catalog of historical droughts and heat waves that have

1144   occurred world-wide.

1145

1146   Turning now to some of the popular metrics of drought, Ped (1975) introduced the index of aridity S_i

1147   defined as

1148 $$S_i = \frac{\Delta T}{\sigma_T} - \frac{\Delta P}{\sigma_P},$$ (B1)

1149   where ΔT and ΔR are the deviations (from a long term mean) of monthly mean air temperatures and

1150   precipitation, and σ_T and σ_P are their standard deviations. This index has been used frequently in the

1151   CIS for identification of atmospheric drought in terms of three classes: light ($0 \leq S_i < 2.0$), average ($2.0 \leq$

1152 $S_i < 3.0$), and strong ($S_i \geq 3.0$).

1153

1154   Another popular index is the hydrothermal coefficient (HTC) developed by Selyaninov (1928).

1155 $$HTC = \frac{\sum R}{0.1 \sum T},$$ (B2)

1156 where the numerator is the total rainfall over the growing season (in mm) and the sum in the

1157 denominator is the accumulated mean daily surface air temperature above 10°C for the same time

1158 period.   The threshold for drought is typically HTC values less than or equal to 0.8, with severe

1159 droughts having HTC values of 0.4 or less.

1160

1161 Meshcherskaya and Blazhevich (1997) developed a combined drought and excessive moisture index

1162 (DM) that takes into account the areal extent of the precipitation and temperature anomalies. Drought

1163 (excessive wet) conditions are defined according to whether the precipitation falls below (exceeds)

1164 80% (120%) of the long term mean, and the temperature anomalies are above (below) 1°C (-1°C).

1165 They produced a catalog of drought occurrence over the main grain producing regions of the FSU for

1166 May-July 1891-1995 for both the European and Asian parts (see their Table 4). They found that the

1167 most severe droughts (in order of decreasing severity) in the European region occurred during 1936,

1168 1975, 1979, and 1891, while for the Asian part the most severe droughts occurred during 1955, 1965,

1169 1951, and 1931.

1170

1171 Dai (2011) compared different forms of the PDSI, finding generally little difference between four

1172 different formulations. They generally compare well with monthly soil moisture observations

1173 (Robock et al 2000), annual streamflow and monthly GRACE satellite-observed water storage

1174 changes. For example, correlations of up to 0.77 were found in parts of the FSU for soil moisture in

1175 the top 1m even over high latitude cold regions (east of the Urals).

1176

1177 Another more recently developed drought index that includes the effects of temperature on drought

1178 variability is the standardized precipitation evapotranspiration index (SPEI, Vicente-Serrano et al. 2010).

1179 The SPEI, similar to the sc-PDSI (Wells et al. 2004), can capture increases in drought severity associated

1180 with higher water demand as a result of evapotranspiration, under global warming conditions. The SPEI was

1181 used for example by Potop and Možny (2011) to study the evolution of drought in the Czech Republic. They

1182 found that increasing temperatures played a role in the intensification of the droughts during the 1980s and

1183 1990s.

1184

1185 Rocheva (2012) proposed a 500mb height index as an indicator of drought over the main grain-

1186 producing regions of Russia using NCEP/NCAR reanalysis data.   They found that droughts occurred

1187 during 1972, 1975, 1979, 1981, 1995, and 1998 (they note that their findings are consistent with the

1188 droughts identified by Strashnayaa and Bogomolova, 2005).

1189

1190 According to Golubev and Dronin (2004), droughts in Russia during the last hundred years tended to

1191 occur over three main geographical areas consisting of Central, Southern and Eastern Russia (based

1192 on the work of Anon, 1933). The central type of drought covers the Volga basin, the Northern

1193 Caucasus and the central chernozem region and some oblasts of the central region, affecting the major

1194 agricultural regions of Russia, and the forest zone of European Russia (associated with numerous

1195 forest fires in the central and northern regions). The southern type of drought is limited to the Volga

1196 basin and Urals region, and while it covers less area, its intensity has generally been more severe and

1197 has often destroyed the entire crop production of the affected region. They note that the eastern type of

1198 drought affects the steppe and forest-steppe of Siberia and this usually occurs when the southern part

1199 of European Russia is characterized by good weather. This again highlights the juxtaposition of

1200 drought and wet conditions as a characteristic feature of climate variability over Eurasia – in this case

1201 the contrast is between European and Asian Russia. Golubev and Dronin (2004) summarize the past

1202   occurrence of each type of drought with the central droughts occurring during 1920, 1924, 1936,

1203   1946, 1972, 1979, 1981 and 1984, the southern droughts occurring during 1901, 1906, 1921, 1939,

1204   1948, 1951, 1957, 1975, 1995, and the eastern droughts occurring during 1911, 1931, 1963, 1965,

1205   1991. One of the worst modern droughts over ER occurred in the summer of 1972 (Fedorov 1973;

1206   Buchinsky 1976). That drought was associated with an anticyclone that was centered over Moscow

1207   and that established in May and persisted throughout the summer. The drought appears to have

1208   started in eastern Ukraine and was at the time characterized as a 100-year event.

1209

1210   A NOAA team of experts[12] note that western Russia has a climatological vulnerability to blocking (see

1211   also Tyrlis and Hoskins 2008; Woollings et al. 2008; Dole et al. 2011) and associated heat waves (e.g.,

1212   1960, 1972, 1988). They point out, however, that a high index value for blocking days is not a

1213   necessary condition for high July surface temperature over western Russia—e.g., the warm summers

1214   of 1981, 1999, 2001, and 2002 did not experience an unusual number of blocking days.

1215

1216   Almaty (2006) found that hydrological drought (low runoff) occurred in the western regions of

1217   Kazakhstan during 1933-1939, 1972-78 and 1996-97. The latter two periods were also low-water

1218   periods in northern Kazakhstan, while 1963-65, 1967-70 and 1996-2000 were low-water periods in

1219   central Kazakhstan. Drought comes to the lowland of southern Kazakhstan roughly every 4-5 years.

1220   It was in drought during 2000-2001 with the Chardarya reservoir having the lowest water storage

1221   since 1977 in August of 2001.

1222

---

[12] http://www.esrl.noaa.gov/psd/csi/events/2010/russianheatwave/prelim.html

References

1223
1224

1225 Adler, R.F., G.J. Huffman, A. Chang, R. Ferraro, P. Xie, J. Janowiak, B. Rudolf, U. Schneider, S.

1226   Curtis, D. Bolvin, A. Gruber, J. Susskind, and P. Arkin, 2003: The Version 2 Global

1227   Precipitation Climatology Project (GPCP) Monthly Precipitation Analysis (1979-Present).

1228   J. Hydrometeor., 4, 1147-1167.

1229

1230 Alexander,L. V., et al. (2006), Global observed changes in daily climate extremes of temperature

1231   and precipitation, J. Geophys. Res., 111, D05109, doi:10.1029/2005JD006290.

1232

1233 Almaty, 2006: Drought Management and Mitigation Assessment for Kazakhstan, Phase Two:

1234   Regional Vulnerability and Capacity Assessment Survey. Nature Protection Ministry

1235   Republic of Kazakhstan, Kazgidromet.

1236

1237 Ambrizzi, T., B. J. Hoskins, and H.-H. Hsu, 1995: Rossby wave propagation and teleconnection

1238   patterns in the austral winter. *J. Atmos. Sci.,* **52,** 3661–3672.

1239

1240 Anon. (1933) Experience of Preliminary Analysis: Eight Catastrophic Droughts over the Last

1241   Forty Years, Part 1, TsUEG, Moscow (in Russian)   or   "TsUEG (1933) Opyt

1242   predvaritelnogo analiza vosmi katastrophicheskix zasyx za poslednii sorok let (Experience

1243   of preliminary analysis of the eight catastrophic droughts for the last forty years), Part 1.

1244   TsUEG, Moscow In Russian)"

1245

1246 Bacmeister, J.T., M.J. Suarez, and F.R. Robertson, 2006: Rain re-evaporation, boundary-

1247   layer/convection interactions and Pacific rainfall patterns in an AGCM, *J. Atmos. Sci*., 8,

1248   SRef-ID: 1607-7962/gra/EGU06-A-08925.

1249

1250 Barash S.I., 1989: History of Bad Harvests and Weather in Europe, Gidrometeoizdat Publ., Leningrad,

1251   236 pp. (in *Russian***).**

1252

1253 Barlow, M., B. Zaitchik, S. Paz, E. Black, J. Evans, A. Hoell, 2013: Drought in the Middle East

1254   and Southwest Asia. J. Climate, to be submitted to the GDIS special collection.

1255

1256 Barriopedro, D., E. M. Fischer, J. Luterbacher, R. M. Trigo, R. Garcia-Herrera, 2011**: The Hot

1257   Summer of 2010: Redrawing the Temperature Record Map of Europe**. *Science*, 2011;

1258   DOI: 10.1126/science.1201224

1259

1260 Batima P., Natsagdorj L., Gombluudev P., Erdenetsetseg B., 2005: Observed Climate Change in

1261   Mongolia. Assessments of Impacts and Adaptations to Climate Change (AIACC)

1262   Working Paper No.12 June 2005. *An electronic publication of the AIACC project*

1263   *available form www.aiaccproject.org*

1264

1265 Bian, H., M. Chin, R. Kawa, B. Duncan, A. Arellano Jr., and R. Kasibhatla, 2007: Uncertainty of

1266   global CO simulations constraint by biomass burning emissions. *J. Geophys. Res.*, 112,

1267   D23308, doi:10.1029/2006JD008376

1268

1269   Bloom, S., L. Takacs, A. DaSilva, and D. Ledvina, 1996: Data assimilation using incremental

1270   analysis updates. *Mon. Wea. Rev.*, **124**, 1256-1271.

1271

1272   Boken,V., A.P. Cracknell, R. L. Heathcote (Eds.), 2005: *Monitoring and predicting agricultural*

1273   *drought: A global study*. Oxford University Press, New York, 472 pp.

1274

1275   Bogolepov, V.A. 1922: *Causes of poor harvest and starvation in Russia in the historical period.*

1276   Publ.House NKZ "Novaya Derevnya", Moscow, 38 pp. (in Russian).

1277

1278   Borisenkov E. P., Pasetsky V. M., 1988: Thousand-year chronicle of unusual phenomena of

1279   nature. "Mysl" Publ., Moscow, 522 pp. (in Russian)

1280

1281   Bothe, O., K. Fraedrich and X. Zhu, 2010: The large-scale circulations and summer drought and

1282   wetness on the Tibetan plateau. Int. J. Climatol., 30, 844-855.

1283

1284   Briffa, K.R., P.D. Jones, F.H. Schweingruber, S.G. Shiyyatov, and E.R. Cook, 1995: Unusual

1285   twentieth-century summer warmth in a 1,000-year temperature record from Siberia.

1286   Letters to Nature, 376, 156- 159.

1287

1288   Buchinsky, I. E. 1976: *Droughts and Dry Winds* (in Russian). Gidrometeoizdat, 214 pp.

1289

1290   Chen, M., P. Xie, J. E. Janowiak, and P. A. Arkin, 2002: Global Land Precipitation: A 50-yr

1291   Monthly Analysis Based on Gauge Observations, J. of Hydrometeorology, 3, 249-266.

1292

1293   Cherenkova, E.A., 2007: Dynamics of Severe Atmospheric Droughts in European Russia.

1294   Russian Meteorology and Hydrology, Vol., 32, No. 11, pp. 675-682. Original Russian text

1295   published in Meteorologiya i Gidrologiya, No. 11, pp. 14-25.

1296

1297   Cherenkova, E.A., 2012: Analysis of extensive atmospheric droughts features in the south of

1298   European Russia. Arid Ecosystems, Vol. 2, No. 4, Pleiades Publishing, Ltd., pp. 209-215.

1299

1300   Chin, M., P. Ginoux, S. Kinne, O. Torres, B. N. Holben, B. N. Duncan, R. V. Martin, J. A.

1301   Logan, A. Higurashi, and T. Nakajima, 2002: Tropospheric aerosol optical thickness from

1302   the GOCART model and comparisons with satellite and sun photometer measurements, *J.*

1303   *Atmos. Sci.*, 59, 461-483

1304

1305   Colarco, P., A. da Silva, M. Chin and T. Diehl, 2009: Online simulations of global aerosol

1306   distributions in the NASA GEOS-4 model and comparisons to satellite and ground-based

1307   aerosol optical depth. *J. Geophys. Res.*, 115, D14207, doi:10.1029/2009JD012820

1308

1309   Collins, N., G. Theurich, C. DeLuca, M. Suarez, A. Trayanov, V. Balaji, P. Li, W. Yang, C. Hill,

1310   and A. da Silva, 2005: Design and implementation of components in the Earth System

1311   Modeling Framework. *Int. J. High Perf. Comput. Appl.*, 19, 341-350, DOI:

1312   10.1177/1094342005056120.

1313

1314   Dai, A. (2011), Characteristics and trends in various forms of the Palmer Drought Severity Index

1315   during 1900–2008, J. Geophys. Res., 116, D12115, doi:10.1029/2010JD015541.

1316

1317   De Beurs, K.M. and G.M. Henebry, 2008: Northern Annular Mode Effects on the Land Surface

1318   Phenologies of Northern Eurasia, J. Climate, 21 4257- 4279.

1319

1320   Dee, D.P., and Coauthors, 2011a: The ERA-Interim reanalysis: Configuration and performanceof

1321   the data assimilation system. *Q. J. R. Meteorol. Soc.*, **137**, 553-597.

1322

1323   Dee, D., P. Poli, and A.J. Simmons, 2011b: Extension of the ERA-Interim reanalysis to 1979.

1324   *ECMWF Newsletter No 128*, Summer 2011, p.7.

1325

1326   Demenzo D. Yu. And I.V. Golovanova, 2007: Climatic changes in the Urals over the past

1327   millennium – an analysis of geothermal and meteorological data, Clim. Past, 3, 237–242,

1328   2007, www.clim-past.net/3/237/2007/

1329

1330   Deser, C., Tomas, R. A. and Peng, S. 2007. The transient atmospheric circulation response to

1331   north Atlantic SST and sea ice anomalies. *J. Climate* **20**, 4751–4767

1332

1333   Ding, Q., and B. Wang, 2005: Circumglobal Teleconnection in the Northern Hemisphere

1334   Summer. *J. Climate*, **18**, 3483-3505.

1335

1336   Ding, Q., and B. Wang, 2007: Intraseasonal Teleconnection between the Summer Eurasian Wave

1337   Train and the Indian Monsoon. J. Climate, 20, 3751-3767.

1338

1339   Dole, R., M. Hoerling, J. Perlwitz, J. Eischeid, P. Pegion, T. Zhang, X.-W. Quan, T. Xu, and D.

1340   Murray (2011), Was there a basis for anticipating the 2010 Russian heat wave?, *Geophys.*

1341   *Res. Lett.*, 38, L06702, doi:10.1029/2010GL046582.

1342

1343   Fan, Y. and H. van den Dool, 2008: A global monthly land surface air temperature analysis for

1344   1948-present. J. Geophys. Res., 113, D01103, doi:10.1029/2007JD008470.

1345

1346   Farat, R.; Kepinska - Kasprzak, M.; Kowalczak, P.; and Mager, P., "Droughts in Poland, 1951-

1347   90" (1998). *Drought Network News (1994-2001).* Paper 42.

1348   http://digitalcommons.unl.edu/droughtnetnews/42

1349

1350   Fedorov, E. K., 1973: *Weather and Yield* (in Russian). Gidrometeoizdat, 55 pp.

1351

1352   Ferranti, L., and P. Viterbo, 2006: The European Summer of 2003: Sensitivity to Soil Water

1353   Initial Conditions. *J. Climate* 19, 3659–3680.

1354

1355   Fischer, E. M., S. I. Seneviratne, P. L. Vidale, D. Lüthi, C. Schär, 2007: Soil Moisture–

1356   Atmosphere Interactions during the 2003 European Summer Heat Wave. *J. Climate*, **20**,

1357   5081–5099. doi: 10.1175/JCLI4288.1.

1358

1359   Francis, J.A. and S. J. Vavrus, 2012: Evidence linking Arctic amplification to extreme weather in

1360   mid-latitudes. Geophys. Re. Let.. 39, L06801, doi:10.1029/2012GL051000, 2012.

1361

1362 Frey, K.E. and L. C. Smith, 2003: Recent temperature and precipitation increases in west Siberia

1363   and their association with the Arctic Oscillation. Polar Research, 22(2), 287-300.

1364

1365 Frich, P., L. V. Alexander, P. Della-Marta, B. Gleason, M. Haylock, A. M. G. Klein Tank, T.

1366   Peterson, 2002: Observed coherent changes in climatic extremes during the second half

1367   of the twentieth century, Clim. Res., Vol. 19: 193–212, 2002

1368

1369 Galos, B., P. Lorenz and D. Jacob, 2007: Will dry events occur more often in Hungary in the

1370   Future? Environ. Res. Lett., 2, 034006, 9pp, doi:10.1088/1748-9326/2/3/034006.

1371

1372 Galarneau, Thomas J., Thomas M. Hamill, Randall M. Dole, Judith Perlwitz, 2012: A Multiscale

1373   Analysis of the Extreme Weather Events over Western Russia and Northern Pakistan during July

1374   2010. *Mon. Wea. Rev.*, **140**, 1639–1664. doi: http://dx.doi.org/10.1175/MWR-D-11-00191.1

1375

1376 Gershunov A. and H. Douville, 2008: Extensive summer hot and cold extremes under current and

1377   possible future climatic conditions: Europe and North America. In: H. F. Diaz and R. J.

1378   Murnane (Eds.), *Climate Extremes and Society.* Cambridge University Press, New York,

1379   348pp, 74-98.

1380

1381 Ghelli, A., A. Garcia-Mendez, F. Prates, and M. Dahoui 2011: Extreme weather events in

1382   summer 2010: how did the ECMWF forecasting systems perform? *ECMWF Newsletter*

1383   Number 125, Autumn 2010

1384

1385   Golubev, G. and N. Dronin, 2004: Geography of Droughts and Food Problems in Russia (1900-

1386   2000). Department of Geography, Moscow State University, Moscow, Russia. Published

1387   by the Center for Environmental Systems Researxh, Kassel, Germany

1388

1389   Groisman, P.Ya., Karl, T.R., Easterling, D.R., Knight, R.W., Jamason, P.B., Hennessy, K.J.,

1390   Suppiah, R, Page, Ch.M., Wibig, J., Fortuniak, K., Razuvaev, V.N., Douglas, A., Førland,

1391   E.,and Zhai, P.-M. 1999: Changes in the probability of heavy precipitation: Important

1392   indicators of climatic change. *Climatic Change,* **42,** No.1, 243-283.

1393

1394   Groisman, P.Ya., and Co-Authors, 2007: Potential forest fire danger over Northern Eurasia:

1395   Changes during the 20th century. *Global and Planetary Change*, **56**, issue 3-4, 371-386.

1396
1397   Groisman and coauthors, 2009: The Northern Eurasian Earth Science Partnership. An example of

1398   science applied to societal needs. Bull. Amer. Meteor. Soc., 671-688.

1399

1400   Groisman, P.Ya., R.W. Knight, and O.G. Zolina, 2013: Recent trends in regional and global

1401   extreme precipitation patterns. Chapter 5.03 in Pielke, R. Sr., Hossain F., et al. (eds)

1402   W*ater Encyclopedia (Elsevier Sciences) Climate Vulnerability: Understanding and*

1403   *Addressing Threats to Essential Resources*. Elsevier Publishing House, ISBN

1404   9780123847034. 1440 pp.

1405

1406   Gumilev, L.N., 1960: *The Huns*. *Central Asia in Ancient Times*. Moscow: Izdatel'stvo Vostochnoi

1407   Literatury (IVL), 1960. First Edition. 290 pp. (in Russian)..

1408

1409   Hess, M., P. Koepke, and I. Schult, 1998: Optical properties of aerosols and clouds: The software

1410   package OPAC, *Bull.Amer.Met.Soc.*, 79, 831-844.

1411

1412   Hirschi, M., S.I. Seneviratne, V. Alexandrov, F. Boberg, C. Boroneant, O.B. Christensen, H.

1413   Formayer, B. Orlowsky, and P. Stepanek, 2011: Observational evidence for soil-moisture

1414   impact on hot extremes in southeastern Europe. Nature Geoscience, 4 (17-21),

1415   doi:10.1038/ngeo1032

1416

1417   Ionita, M., G. Lohmann, N. Rimbu, S. Chelcea, M. Dima, 2012: Interannual to decadal summer

1418   drought variability over Europe and its relationship to global sea surface temperature,

1419   Clim Dyn (2012) 38:363–377, DOI 10.1007/s00382-011-1028-y

1420

1421   IPCC, 2001: *Third Assessment Report of the Intergovernmental Panel on Climate Change.*

1422   *Chapter 2: Observed Climate Variability and Change* [C.K. Folland, T.R. Karl,

1423   coordinating lead authors].

1424

1425   IPCC, 2007a: *Climate Change 2007: The Physical Science Basis. Contribution of Working Group*

1426   *I to the Fourth Assessment Report of the Intergovernmental Panel on Climate Change*

1427   [Solomon, S., D. Qin, M. Manning, Z. Chen, M. Marquis, K.B. Averyt, M.Tignor and

1428   H.L. Miller (eds.)]. Cambridge University Press, Cambridge, United Kingdom and New

1429   York, NY, USA.

1430

1431   IPCC, 2007b: *Climate Change 2007: Working Group II: Impacts, Adaptation and Vulnerability.* [M.L.

1432   Parry, O.F. Canziani, J.P. Palutikof, P.J. van der Linden and C.E. Hanson, Eds.] Cambridge

1433   University Press, Cambridge, UK, 976 pp.

1434

1435   IPCC, 2012: Managing the Risks of Extreme Events and Disasters to Advance Climate Change

1436   Adaptation. A Special Report of Working Groups I and II of the Intergovernmental Panel on

1437   Climate Change [Field, C.B., V. Barros, T.F. Stocker, D. Qin, D.J. Dokken, K.L. Ebi, M.D.

1438   Mastrandrea, K.J. Mach, G.-K. Plattner, S.K. Allen, M. Tignor, and P.M. Midgley (eds.)].

1439   Cambridge University Press, Cambridge, UK, and New York, NY, USA, 582 pp.

1440

1441   Johansson, Åke, 2007:Prediction skill of the NAO and PNA from daily to seasonal time scales.

1442   J. Climate, 20, 1957 – 1975.

1443

1444   Jones, P.D., Lister, D.H., Osborn, T.J., Harpham, C., Salmon, M. and Morice, C.P., 2012:

1445   Hemispheric and large-scale land surface air temperature variations: an extensive revision

1446   and an update to 2010. *Journal of Geophysical Research*, doi:10.1029/2011JD017139.

1447

1448   Kahan, A., 1989: Russian Economic History: The Nineteenth Century. Roger Weiss, Ed., The

1449   University of Chicago Press, pp251.

1450

1451   Kleshenko, A.D., et al., 2005: Monitoring Agricultural Drought in Russia. A. D. Kleshenko,

1452   E.K. Zoidze, V. K. Boken, in "Monitoring and Predicting Agricultural Drought", V.

1453   Boken, A.P. Cracknell, R. L. Heathcote (eds.), Oxford University Press, New York. 472

1454   pp.

1455

1456   Körnich, H., 2010: Predictability of the coupled troposphere-stratosphere system. ECMWF

1457   Seminar on Predictability in the European and Atlantic regions, 6 to 9 September 2010.

1458

1459   Koster, R.D., M.J. Suárez, A. Ducharne, M. Stieglitz, and P. Kumar, 2000: A catchment-based

1460   approach to modeling land surface processes in a GCM, Part 1, Model Structure. *J.*

1461   *Geophys. Res.*, 105, 24809- 24822.

1462

1463   Koster, R.D., P.A. Dirmeyer,Zh. Guo,G. Bonan,E. Chan,P. Cox,C. T. Gordon,S. Kanae,E.

1464   Kowalczyk, D. Lawrence, P. Liu, C-H. Lu, S. Malyshev, B. McAvaney, K. Mitchell, D.

1465   Mocko, T. Oki, K. Oleson, A. Pitman, Y. C. Sud, C. M. Taylor, D. Verseghy, R. Vasic, Y.

1466   Xue, and T. Yamada, 2004: Regions of Strong Coupling Between Soil Moisture and

1467   Precipitation. Science, 305, 1138-1140

1468

1469   Koster, R. D., B. M. Fekete, G. J. Huffman, and P. W. Stackhouse Jr. (2006a), Revisiting a

1470   hydrological analysis framework with International Satellite Land Surface Climatology

1471   Project Initiative 2 rainfall, net radiation, and runoff fields, J. Geophys. Res., 111,

1472   D22S05, doi:10.1029/2006JD007182.

1473

1474   Koster, R. D., M. J. Suarez, and S. D. Schubert, 2006b: Distinct hydrological signatures in

1475   observed historical temperature fields. J. Hydromet., 7, 1061-1075.

1476

1477   Koster, R., and S. P. Mahanama, 2012. Land-surface controls on hydroclimatic means and

1478   variability. *J*. *Hydrometeorol*., 13, 1604-1620. doi: 10.1175/JHM-D-12-050.1.

1479

1480   Lau, William K. M., Kyu-Myong Kim, 2012: The 2010 Pakistan Flood and Russian Heat Wave:

1481   Teleconnection of Hydrometeorological Extremes. *J. Hydrometeor*, 13, 392–403. doi:

1482   http://dx.doi.org/10.1175/JHM-D-11-016.1

1483

1484   *Lin*, Shian-Jiann, *2004*: A "Vertically Lagrangian" Finite-Volume *Dynamical Core* for Global

1485   Models. Mon. Wea. Rev., 132, 2293–2307.

1486

1487   Liu, Alan Z., Mingfang Ting, Hailan Wang, 1998: Maintenance of Circulation Anomalies during

1488   the 1988 Drought and 1993 Floods over the United States. *J*. *Atmos*. *Sci*., **55**, 2810–2832.

1489

1490   Lorenz, R., E. B. Jaeger, S.I. Seneviratne, 2010: Persistence of heat waves and its link to soil

1491   moisture Memory. Geophys.Res.Let., 37, 9, DOI:10.1029/2010GL042764.

1492

1493   Lupo, Anthony R., Igor I.Mokhov, Merseid G. Akperov, Alexander V. Chernokulsky, and H.

1494   Athar, 2012: A Dynamic Analysis of the Role of the Planetary- and Synoptic-Scale in the

1495   Summer of 2010 Blocking Episodes over the European Part of Russia. Hindawi

1496   Publishing Corporation, Advances in Meteorology, Volume 2012, Article ID 584257, 11

1497   pages doi:10.1155/2012/584257

1498

1499   Lydolph, P.E., 1964: Russian Sukhovey. *Annals of Assoc. Amer. Geograph*., **54**, No. 3, 291-309.

1500

1501	Lyon, B. F., and R. M. Dole, 1995: A comparative study of the intense summer heat

1502	wave/droughts of 1980 and 1988. *J. Climate,* **8,** 1658-1676.

1503

1504	Matsueda, M., 2011: Predictability of Euro-Russian blocking in summer of 2010. *Geophy. Res.*

1505	*Lett.*, 38, L06801, doi:10.1029/2010GL046557

1506

1507	Meehl, G., and C. Tebaldi, 2004: More intense, more frequent and longer lasting heat waves in

1508	the 21st century. *Science*, 305, 994–997.

1509

1510	Meshcherskaya, A.V., and V.G. Blazhevich, 1997: The drought and excessive moisture indices in

1511	a historical perspective in the principal grain-producing regions of the Former Soviet

1512	Union. *J. Climate,* **10,** 2670-2682.

1513

1514	Meshcherskaya A.V., M.P. Golod and V.M. Mirvis, 2011: The drought in 2010 against the

1515	background of multiannual changes in aridity in the major grain producing regions of the

1516	European part of Russia. *Proc. Main Geophys. Observatory*, **563**, 1-27 (in Russian).

1517

1518	Meinshausen, M., S. J. Smith, K. V. Calvin, J. S. Daniel, M. L. T. Kainuma, J.-F. Lamarque, K.

1519	Matsumoto, S. A. Montzka, S. C. B. Raper, K. Riahi, A. M. Thomson, G. J. M. Velders

1520	and D. van Vuuren, 2011: "The RCP Greenhouse Gas Concentrations and their Extension

1521	from 1765 to 2300." *Climatic Change* (Special Issue), DOI: 10.1007/s10584-011-0156-z.

1522

1523   Mokhov I.I., 2011: Specific features of the 2010 summer heat formation in the European territory

1524   of Russia in the context of general climate changes and climate anomalies. *Izvestiya,*

1525   *Atmos. Oceanic Phys.*, **47**(6), 653-660.

1526

1527   Moorthi, S., and M.J. Suarez, 1992: Relaxed Arakawa-Schubert, A Parameterization of Moist

1528   Convection for General-Circulation Models. *Mon. Wea. Rev.* 120, 978-1002

1529

1530   Mueller, B., and S.I. Seneviratne, 2012: Hot days induced by precipitation deficits at the global

1531   scale. ***Proc. Natl. Acad. Sci.***, 109 (31), 12398-12403, doi: 10.1073/pnas.1204330109.

1532

1533   Nakamura, H., M. Nakamura, and J. L. Anderson, 1997: The role of high- and low-frequency

1534   dynamics and blocking formation. *Mon. Wea. Rev.,* **125,** 2074–2093.

1535

1536   Nandintsetseg, B., J.S. Greene, and C.E. Goulden, 2007: Trends in extreme daily precipitation and

1537   temperature near Lake Hövsgöl, Mongolia. *Int. J. Climatol.*, 27, 341-347.

1538

1539   Nascimento, E. L., and T. Ambrizzi, 2002: The influence of atmospheric blocking on the Rossby

1540   wave propagation in Southern Hemisphere winter flows. J. Meteor. Soc. Japan, 80, 139-

1541   159.

1542

1543   Nesterov, V.G. 1949. Combustibility of the forest and methods for its determination, USSR State

1544   Industry Press (in Russian).

1545

1546   Obukhov, A.M., M.V. Kurganskii, and M.S. Tatarskaya, 1984: Dynamical conditions of drought

1547   and other large-scale weather anomalies formation. Meteorol. Gidrol, No. 10. [Sov.

1548   Meteorol. Hydrol., No. 10, 1984].

1549

1550 Otto, F. E. L., N. Massey, G. J. van Oldenborgh, R. G. Jones, and M. R. Allen (2012),

1551   Reconciling two approaches to attribution of the 2010 Russian heat wave*, Geophys. Res.*

1552   *Lett., 39, L04702, doi:10.1029/2011GL050422.*

1553

1554 Pawson, S., R. S. Stolarski, A. R. Douglass, P. A. Newman, J. E. Nielsen, S. M. Frith, and M. L.

1555   Gupta, 2008: Goddard Earth Observing System chemistry-climate model simulations of

1556   stratospheric ozone-temperature coupling between 1950 and 2005. *J. Geophys. Res.*, 113,

1557   D12103, doi:10.1029/2007JD009511.

1558

1559 Ped, D.A., 1975: On indicators of droughts and wet conditions (in Russsian). Proc. USSR

1560   Hydrometeor. Centre, 156, 19-39.

1561

1562 Pines, Yu., 2012: *The Everlasting Empire: The Political Culture of Ancient China and Its Imperial*

1563   *Legacy.* Princeton University Press, - 248 pp.

1564

1565 Polozova, L.G. and A.A. Grigoryeva, 1984: Role of circulation factor in formation of dry periods,

1566   Helio-physical factors of weather and climate. Proceedings of the A.I. Voeikov Main

1567   Geophysical Observatory, Vyp. 471, pp. 50-54 [Infuence of features of circulation of an

1568   atmosphere on occurrence of droughts].

1569

1570 POTOP, V. – MOŽNÝ, M. Podtyp: Příspěvek ve sborníku (mimo kategorie RIV); The

1571 application a new drought index - standardized precipitation evapotranspiration index in

1572 the Czech Republic. 2011. In: Středová, H., Rožnovský, J., Litschmann, T. (eds):

1573 Mikroklima a mezoklima krajinných struktur a antropogenních prostředí. Skalní mlýn, 2.–

1574 4.2.2011, 12 s. ISBN 978-80-86690-87-2 (CD).

1575

1576 Protserov, A.V. (1950) Drought on European Territory of the Soviet Union: Agroclimatic

1577 Conditions of Steppes of the Ukrainian SSR and Ways to Improve Them. Academy of

1578 Sciences of the Ukrainian SSR, Kiev, p. 17-22 (in Russian)

1579

1580 Rahmstorf, S. and D. Coumou, 2011: Increase of extreme events in a warming world. Proc. Natl.

1581 Acad. Sci. U.S.A., vol. 108 no. 44, 17905-17909, doi: 10.1073/pnas.1101766108.

1582

1583 Rayner, N. A.; Parker, D. E.; Horton, E. B.; Folland, C. K.; Alexander, L. V.; Rowell, D. P.;

1584 Kent, E. C.; Kaplan, A., 2003. Global analyses of sea surface temperature, sea ice, and

1585 night marine air temperature since the late nineteenth century, J. Geophys. Res., Vol. 108,

1586 No. D14, 4407 10.1029/2002JD002670.

1587

1588 Richman M.B., 1986. Rotation of principal components. J. Climatol., 6, 293–335.

1589

1590 Rienecker, M.M., M.J. Suarez, R. Todling, J. Bacmeister, L. Takacs, H.-C. Liu, W. Gu, M.

1591 Sienkiewicz, R.D. Koster, R. Gelaro, I. Stajner, and E. Nielsen, 2008: *The GEOS-5 Data*

1592 *Assimilation System- Documentation of Versions 5.0.1, 5.1.0, and 5.2.0*. Technical Report

1593   Series on Global Modeling and Data Assimilation, NASA/TM-2007-104606, M.J. Suarez,

1594   Ed., Vol. 27, 95 pp.

1595

1596 Rienecker M.M., and coauthors, 2011. MERRA - NASA's Modern-Era Retrospective Analysis

1597   for Research and Applications. *J. Climate,* e-View doi: 10.1175/JCLI-D-11-00015.1

1598

1599 Robock, Alan, Konstantin Y. Vinnikov, Govindarajalu Srinivasan, Jared K. Entin, Steven E.

1600   Hollinger, Nina A. Speranskaya, Suxia Liu, and A. Namkhai, 2000: The Global Soil

1601   Moisture Data Bank. *Bull. Amer. Meteorol. Soc.*, **81**, 1281-1299.

1602

1603 Robock, Alan, Mingquan Mu, Konstantin Vinnikov, Iryna V. Trofimova, and Tatyjana I.

1604   Adamenko, 2005: Forty five years of observed soil moisture in the Ukraine: No summer

1605   desiccation (yet). *Geophys. Res. Lett.*, **32**, L03401, doi:10.1029/2004GL021914.

1606

1607 Rocheva, E.V., 2012: Possible forerunners of droughts in agricultural areas of Russia. Russian

1608   Meteorology and Hydrology, vol. 37, no. 9, pp. 575-585. Original Russian published in

1609   Meteorologiya i Gidrologiya, no. 9, 5-18.

1610

1611 Rudenko, A. I., Ed., 1958: Droughts in the USSR. Their Origin, Frequency of Occurrence and

1612   Impact on Yield (in Russian). Gidrometeoizdat, 206 pp.

1613

1614 Sato N., and Takahashi M. 2006: Dynamical processes related to the appearance of quasi-

1615   stationary waves on the subtropical jet in the midsummer northern hemisphere. *Journal of*

1616   *Climate* **19**: 1531–1544, DOI: 10.1175/JCLI3697.1.

1617

1618   Scaife, A.A., Wollings, T., Knight, J., Martin G. and Hinton, T. 2010. Atmospheric blocking and

1619   mean biases in climate models. *Journal of Climate* **23**: 6143-6152.

1620

1621   Schneidereit, Andrea, Silke Schubert, Pavel Vargin, Frank Lunkeit, Xiuhua Zhu, Dieter H. W.

1622   Peters, Klaus Fraedrich, 2012: Large-Scale Flow and the Long-Lasting Blocking High

1623   over Russia: Summer 2010. *Mon. Wea. Rev.*, **140**, 2967–2981.

1624

1625   Schubert, S., D. Gutzler, H. Wang, A. Dai, T. Delworth, C. Deser, K. Findell, R. Fu, W. Higgins,

1626   M. Hoerling, B. Kirtman, R. Koster, A. Kumar, D. Legler, D. Lettenmaier, B. Lyon, V.

1627   Magana, K. Mo, S. Nigam, P. Pegion, A. Phillips, R. Pulwarty, D. Rind, A. Ruiz-

1628   Barradas, J. Schemm, R. Seager, R. Stewart, M. Suarez, J. Syktus, M. Ting, C. Wang, S.

1629   Weaver, N. Zeng, 2009: A USCLIVAR Project to Assess and Compare the Responses of

1630   Global Climate Models to Drought-Related SST Forcing Patterns: Overview and Results,"

1631   J. Climate, 22, 5251–5272.

1632

1633   Schubert, S., H. Wang, and M. Suarez. J., 2011: Warm Season Subseasonal Variability and

1634   Climate Extremes in the Northern Hemisphere: The Role of Stationary Rossby waves,

1635   Climate, 24, 4773-4792, 2011.

1636

1637   Sedláček, J., O. Martius, and R. Knutti (2011), Influence of subtropical and polar sea-surface

1638   temperature anomalies on temperatures in Eurasia, Geophys. Res. Lett., 38, L12803,

1639   doi:10.1029/2011GL047764.

1640

1641   Selianinov, G.T., 1928: On agricultural climate evaluation (in Russian). Proc. Agric., Meteor.,

1642   20, 165-177.

1643

1644   Seneviratne, S.I., D. Lüthi, M. Litschi, and C. Schär, 2006: Land-atmosphere coupling and

1645   climate change in Europe. *Nature*, **443**, 205-209.

1646

1647   Seneviratne, S. I., et al. 2013: J. Climate, to be submitted to the GDIS special collection.

1648

1649   Shver, Ts. A., 1976: *Atmospheric Precipitation over the USSR Territory*, Gidrometeoizdat,

1650   Leningrad, 302 pp. (in Russian).

1651

1652   Sinor, Denis, ed. (1994). *The Cambridge history of early Inner Asia* (1. publ. ed.). Cambridge

1653   [u.a.]: Cambridge Univ. Press. pp. 310–311. ISBN 0-521-24304-1.

1654

1655   Stankūnavičius, G., D. Basharin, and D. Pupienis, 2012: Relationship between Eurasian large-

1656   scale patterns and regional climate variability over the Black and Baltic Seas. Boreal Env.

1657   Res., 17, 327-346.

1658

1659   Stefanon, M., F. D'Andrea and P. Drobinski, 2012 : Heatwave classification over Europe and the

1660   Mediterranean region. *Environ. Res. Lett.* **7** 014023 doi:10.1088/1748-9326/7/1/014023

1661

1662   Strashnaya,A.I. and N.A. Bogomolova, 2005: On the catalog of severe droughts of soils sown

1663   with early spring grain crops in the Chernozem zone of Russia, "Trudy Gidromettsentra

1664   Rossii (Trans. Russ. Hydrometeorol.Res. Center), Issue 340 [in Russian].

1665

1666   Tang, Q., G. Leng, and P. Y. Groisman, 2012: European hot summers associated with a reduction

1667   of cloudiness. *J. Climate*, **25**(10): 3637-3644. doi: 10.1175/JCLI-D-12-00040.1

1668

1669   Tang, Q., and G. Leng, 2012a: Changes in cloud cover, precipitation, and summer temperature in

1670   North America from 1982 to 2009, J. *Climate*, e-View. doi:

1671   http://dx.doi.org/10.1175/JCLI-D-12-00225.1

1672

1673   Tang Q. and G. Leng, 2012b: Damped summer warming accompanied with cloud cover increase

1674   over Eurasia.   From 1982 to 2009. *Environ. Res. Lett.*, **7**, 014004 (7 pp.),

1675   doi:10.1088/1748-9326/7/1/014004

1676

1677   Thompson, D.W.J., and J.M. Wallace, 2001: Regional Climate Impacts of the Northern

1678   Hemisphere Annular Mode. *Science*, **293**, 85-89.

1679

1680   Ting, M. and L. Yu, 1998: Steady response to tropical heating in wavy linear and nonlinear

1681   baroclinic models. *J. Atmos. Sci.*, **55**, 3565–3582.

1682

1683   Trenberth, K.E. and J.T. Fasullo, 2012: Climate extremes and climate change: The Russian heat

1684   wave and other climate extremes of 2010. JOURNAL OF GEOPHYSICAL RESEARCH,

1685   VOL. 117, D17103, doi:10.1029/2012JD018020

1686

1687   Tyrlis, E., B. J. Hoskins, 2008: Aspects of a Northern Hemisphere Atmospheric Blocking Climatology,

1688   *J.* Atmos. Sci., 65, 1638–1652. doi: http://dx.doi.org/10.1175/2007JAS2337.1

1689

1690   Vámbéry, A., 1886: The Story of the Nations: Hungary. With the collaboration of Louis

1691   Heilprin, pp 453, excerpt on page 314. New York, G.P. Putnam's Sons, London: T.

1692   Fisher Unwin

1693

1694   van der Schrier, G., K. R. Briffa, P. D. Jones, T. J. Osborn, 2006: Summer Moisture Variability

1695   across Europe. *J. Climate*, **19**, 2818–2834. doi: http://dx.doi.org/10.1175/JCLI3734.1

1696

1697   Vannari, P.I., 1911: Meteorological networks in Russia and other countries. *Issue of*

1698   *Meteorological Papers in the Memory of the Chief of the Meteorological Committee of*

1699   *Imperator Russian Geography Society A.I. Voeikov*, **1**, 51-64 (in Russian).

1700

1701   Vautard, R., P. Yiou, F. D'Andrea, N. de Noblet, N. Viovy, C. Cassou, J. Polcher, P. Ciais, M.

1702   Kageyama, and Y. Fan (2007), Summertime European heat and drought waves induced by

1703   wintertime Mediterranean rainfall deficit, *Geophys. Res. Lett.*, 34, L07711,

1704   doi:10.1029/2006GL028001.

1705

1706   Vazhov, V. I., 1961: Drought Frequency over the Russian Plain in the historical period. *Rept. of*

1707   *Crimea Dept. of the Russian Geograph. Soc*., Simpheropol, **7**, 5-17 (in Russian).

1708

1709   Vicente-Serrano S.M., Beguería S., López-Moreno J.I.: A Multi-scalar drought index sensitive to

1710   global warming: The Standardized Precipitation Evapotranspiration Index, SPEI. Journal

1711   of Climate 23(7), 1696-1718, 2010. DOI: 10.1175/2009JCLI2909.1

1712

1713   Volodin, E. M., 2011: The nature of some strongest summer heat waves. In: N. P. Shakina, (Ed.),

1714   *Analysis of Abnormal Weather Conditions in Russia in Summer 2010*, Triada, Moscow, 48–57

1715   (in Russian).

1716

1717   Wells, N., Goddard, S., and Hayes, M. J.: A self-calibrating Palmer Drought Severity Index, J.

1718   Climate, 17, 2335   2351, 2004.

1719

1720   Woollings, T. J., B. J. Hoskins, M. Blackburn, and P. Berrisford, 2008: A new Rossby wave-

1721   breaking interpretation of the North Atlantic Oscillation. *J. Atmos. Sci.,* **65,** 536–553.

1722

1723   Wu, Z., J. Li, Z. Jiang, J. He, and X. Zhu, 2012: Possible effects of the North Atlantic Oscillation

1724   on the strengthening relationship between the East Asian summer monsoon and ENSO."

1725   *Int. J. Climatol*., 32, 794-800.

1726

1727   Zampieri, M. *et al*. Hot European summers and the role of soil moisture in the propagation of

1728   Mediterranean drought. J. Clim. 22, 4747–4758 (2009).

1729

1730   Zhang and Zhou, 2013: J. Climate, to be submitted to the GDIS special collection.

1731

1732   Table B1: *Droughts and heat wave years in Eurasia (1875-2012). ENSO phase refers to summer*
1733   *months. Bold indicates major droughts/ heat waves as identified by various authors.*

Year	Months	Regions Affected	Source (s)	Comments
1875		Ukraine, Non-Black Soil Region, North Caucasus	Kahan 1989; Rudenko 1958	General Dmitry Milyutin's diary (see text); Strong La Niña
1879		Drought in middle Volga, central Ukraine	Kahan 1989	La Niña
1885		South and East Ukraine, middle and lower Volga, North Caucasus	Kahan 1989	Tchaikovsky letter [13]
1889		Drought in Ukraine, Lower Volga	Kahan 1989	La Niña
1890		Drought in Central and southern regions of European Russia, Lower Volga, Ural; severe drought in Ukraine	Fedorov 1973; Buchinsky 1976; Kahan 1989; Boken et al. 2005	La Niña
1891	May-August	Drought in Central and southern regions of European Russia, spreading north to middle course of Kama and Vyatka, Blacksoil (Chernozem) Region, all of Volga, Southern Ukraine, North Caucasus, 80% of European Territory of USSR (ETU) between 45-55N; 30-50E affected by drought	Fedorov 1973; Buchinsky 1976; Meshcherskaya and Blazhevich 1997; Kahan 1989; Polozova and Grigoryeva 1984	Absolute temperature record for May was set (+31.8 deg. C), not broken until 2007
1892		Drought in Central and southern regions of European Russia; Ukraine, Central Blacksoil Region, Lower Volga, North Caucasus; 90% of (ETU) between 45-55N; 30-50E affected by drought (Polozova and Grigoryeva 1984)	Fedorov 1973; Buchinsky 1976; Kahan 1989; Polozova and Grigoryeva 1984	La Niña
1897		Drought in South Ukraine, Lower Volga; 80% of (ETU) between 45-55N; 30-50E affected by drought	Kahan 1989; Polozova and Grigoryeva 1984	
1898		Severe drought in Ukraine	Boken et al 2005	
1900		Drought in Ukraine, Western Siberia	Kahan 1989	El Niño
1901		"Southern" type of drought in the Volga River Basin (Volga and Volga-Vyatka) and the Urals Region; eastern Ukraine, Ural, lower and middle Volga; 95% of (ETU) between 45-55N; 30-50E affected by drought	Golubev and Dronin, 2004; Kahan 1989;Polozova and Grigoryeva 1984	
1905		60% of (ETU) between 45-55N; 30-50E affected by drought	Polozova and Grigoryeva 1984	
1906		"Southern" type of drought in the Volga River Basin (Volga and Volga-Vyatka) and the Urals Region; eastern Ukraine, Volga; 75% of (ETU) between 45-55N; 30-50E affected by drought	Golubev and Dronin, 2004; Kahan 1989; Polozova and Grigoryeva 1984	Severe drought in Ukraine
1911		"Eastern" type of drought in-steppe and forest-steppe of Western and Eastern Siberia; European Russia, Ukraine, west Siberia; severe drought in Ukraine; 65% of (ETU) between 45-55N; 30-50E affected by drought	Golubev and Dronin, 2004; Kahan 1989; Boken et al 2005; Polozova and Grigoryeva 1984	La Niña
1914		Volga, Ukraine; 75% of (ETU) between 45-55N; 30-50E affected by drought	Kahan 1989; Polozova and Grigoryeva 1984	El Niño
1917		65% of (ETU) between 45-55N; 30-50E affected by drought	Polozova and Grigoryeva 1984	
1918		Ukraine	Rudenko 1958	
1920		Drought in Central Russia, forest zone of European Russia; Ukraine, Volga; 95% of (ETU) between 45-55N; 30-50E affected by drought	Golubev and Dronin, 2004; Kahan 1989; Polozova and Grigoryeva 1984	
1921		"Southern" type of drought in the Volga River Basin (Volga and Volga-Vyatka) and the Urals Region; European Russia, Ukraine, Volga, Western Siberia; 95% of (ETU) between 45-55N; 30-50E affected by drought	Golubev and Dronin, 2004; Kahan 1989; Rudenko 1958; Polozova and Grigoryeva 1984	1921 Famine in Russia (Volga-Ural region); La Niña; severe drought in Ukraine
1924		Drought in Central Russia, forest zone of European Russia; Central Blacksoil Region, Lower Volga; 90% of (ETU) between 45-55N; 30-50E affected by drought	Golubev and Dronin, 2004; Kahan 1989; Polozova and Grigoryeva 1984	La Niña
1931	July	Heat wave; "Eastern" type of drought in steppe and forest-steppe of Western and Eastern Siberia; Ural, Central Blacksoil Region; 75% of (ETU) between 45-55N; 30-50E affected by drought	NOAA expert team[14]; Golubev and Dronin, 2004; Kahan 1989; Meshcherskaya and Blazhevich 1997; Polozova and Grigoryeva	

---

[13] *(in a letter from Tchaikovsky (composer) to N. von Mekk, 3-10 August 1885, in Majdanovo, now Klin): "I'm writing to you at three o'clock in the afternoon in such darkness, you would think it was nine o'clock at night. For several days, the horizon has been enveloped in a smoke haze, arising, they say, from fires in the forest and peat bogs. Visibility is diminishing by the day, and I'm starting to fear that we might even die of suffocation."* ***http://therese-phil.livejournal.com/171196.html***

[14] http://www.esrl.noaa.gov/psd/csi/events/2010/russianheatwave/prelim.html

				1984
1933-39		Drought (low-water) years in western Kazakhstan	Almaty 2006	
1934		70% of (ETU) between 45-55N; 30-50E affected by drought	Polozova and Grigoryeva 1984	
1936		Drought in Central Russia, forest zone of European Russia; Ukraine, Volga, Western Siberia; 90% of (ETU) between 45-55N; 30-50E affected by drought	Golubev and Dronin, 2004; Meshcherskaya and Blazhevich 1997; Kahan 1989; Polozova and Grigoryeva 1984	Dry preceding winter and spring – Cherenkova 2012
1938		Central Blacksoil Region, Eastern Ukraine; 85% of (ETU) between 45-55N; 30-50E affected by drought	Kahan 1989; Polozova and Grigoryeva 1984	Dry preceding winter and spring – Cherenkova 2012; La Niña
1939		"Southern" type of drought in the Volga River Basin (Volga and Volga-Vyatka) and the Urals Region; Lower Volga, Upper Volga, Southeast Ukraine; 65% of (ETU) between 45-50E affected by drought	Golubev and Dronin, 2004; Kahan 1989; Polozova and Grigoryeva 1984	
1946		Drought in Central Russia, forest zone of European Russia; Ukraine, Central Blacksoil Region, Volga, North Caucasus; 100% of (ETU) between 45-55N; 30-50E affected by drought	Golubev and Dronin, 2004; Kahan 1989; Polozova and Grigoryeva 1984	Famine; serious crop failures in grain production in USSR; drought covered 50% of total agricultural land of USSR
1948		"Southern" type of drought in the Volga River Basin (Volga and Volga-Vyatka) and the Urals Region	Golubev and Dronin, 2004; Kahan 1989	serious crop failures in grain production in USSR
1950		Eastern Ukraine, Middle and Lower Volga; 85% of (ETU) between 45-55N; 30-50E affected by drought	Kahan 1989; Polozova and Grigoryeva 1984	La Niña
1951		"Southern" type of drought in the Volga River Basin (Volga and Volga-Vyatka) and the Urals Region; drought in Asian part of FSU; Ukraine, Lower Volga; 75% of (ETU) between 45-55N; 30-50E affected by drought	Golubev and Dronin, 2004; Meshcherskaya and Blazhevich 1997; Kahan 1989; Polozova and Grigoryeva 1984	El Niño
1953		Ukraine, Volga	Kahan 1989	
1954		Southern Ukraine, Lower Volga; 60% of (ETU) between 45-55N; 30-50E affected by drought	Kahan 1989; Polozova and Grigoryeva 1984	La Niña
1955	July	Heat wave over Russia; drought in Asian part of FSU; western Siberia, Lower Volga	Meshcherskaya and Blazhevich 1997; Kahan 1989	La Niña
1957		"Southern" type of drought in the Volga River Basin (Volga and Volga-Vyatka) and the Urals Region; 75% of (ETU) between 45-55N; 30-50E affected by drought	Golubev and Dronin, 2004; Polozova and Grigoryeva 1984	serious crop failures in grain production in USSR; El Nino
1959		60% of (ETU) between 45-55N; 30-50E affected by drought	Polozova and Grigoryeva 1984	serious crop failures in grain production in USSR
1960		Heat wave in Western Russia	NOAA expert team	Associated with blocking
1963		Eastern" type of drought in steppe and forest-steppe of Western and Eastern Siberia; western Siberia, Kazakhstan, Ural, eastern Ukraine; 95% of (ETU) between 45-55N; 30-50E affected by drought	Golubev and Dronin, 2004; Kahan 1989; Polozova and Grigoryeva 1984	serious crop failures in grain production in USSR; El Nino
1965		Eastern" type of drought in steppe and forest-steppe of Western and Eastern Siberia; drought in Asian part of FSU; western Siberia, Kazakhstan, central Asia, Ural, Volga	Golubev and Dronin, 2004; Meshcherskaya and Blazhevich 1997; Kahan 1989	El Niño
1972-78		Drought (low-water) years in western and northern Kazakhstan	Almaty 2006	
1972	Established in May and lasted through summer	Drought and heat wave: Anticyclone centered over Moscow, covered western Russia, drought started in eastern Ukraine; 100% of (ETU) between 45-55N; 30-50E affected by drought	Fedorov 1973; Buchinsky 1976; Strashnaya and Bogomolova, 2005; Polozova and Grigoryeva 1984; Cherenkova 2012	Blocking, *one of worst modern droughts* - "100-year" drought; El Niño; serious crop failures in grain production in USSR; Dry preceding winter and spring.
1975		"Southern" type of drought in the Volga River Basin (Volga and Volga-Vyatka) and the Urals Region	Golubev and Dronin, 2004; Meshcherskaya and Blazhevich 1997; Strashnaya and Bogomolova, 2005	serious crop failures in grain production in USSR; La Niña
1979		Drought in Central Russia, forest zone of European Russia	Golubev and Dronin, 2004; Meshcherskaya and Blazhevich 1997; Strashnaya and Bogomolova, 2005	serious crop failures in grain production in USSR
1981	July heat wave	Drought and heat wave in Central Russia, forest zone of European Russia	Golubev and Dronin, 2004; Meshcherskaya and Blazhevich 1997; Strashnaya and Bogomolova, 2005; NOAA expert team	No unusual blocking; Worst drought in European Russia between 1891-1995; serious crop failures in grain production in USSR

1984		Drought in Central Russia, forest zone of European Russia, North and west UK	Golubev and Dronin, 2004, *Ben Lloyd-Hughes, Benfield Hazard Research Centre, UCL*	UK: Very dry spring and summer led to the imposition of hosepipe bans.
1988	July	Russia	NOAA expert team	Blocking, La Niña
1991		"Eastern" type drought in steppe and forest-steppe of Western and Eastern Siberia	Golubev and Dronin, 2004;	El Niño
1992		Germany, Hungary, Bulgaria and much of western Russia	*Ben Lloyd-Hughes, Benfield Hazard Research Centre, UCL*	German crop production reduced by 22%. Irrigation suspended in Bulgaria. Worst Russian drought in 10 years
1995		"Southern" type of drought in the Volga basin (Volga and Volga-Vyatka) and the Urals Region	Golubev and Dronin, 2004; Strashnaya and Bogomolova, 2005	El Niño
1996-97		Drought (low-water) years in western and northern Kazakhstan	Almaty 2006	
1998		The Volga Region, North Caucasus and Central-Chernozem, warmest year of the last century for Mongolia	Strashnaya and Bogomolova, 2005, Batima et al. 2005	
1999-2002		Summer drought in Mongolia	Batima et al. 2005	1999, 2000 La Niña ; 2002 El Niño
1999	July	Heat wave in Western Russia	NOAA expert team	No unusual blocking over Russia; La Niña
2001		July heat wave in Western Russia, drought in southern Kazakstan	NOAA expert team, Almaty 2006	No unusual blocking over Russia
2002	July	July heat wave in Western Russia, drought in southern Kazakhstan	NOAA expert team, Almaty 2006	No unusual blocking over Russia
2007	May, June, continued to September in Japan	Heat wave in Southeast Europe (June-August), South Asian countries of India, Pakistan, Bangladesh and Nepal, as well as Russia, Japan and China	.Buranov, Ivan, Geroyeva, Anna, Kornysheva, Alyona (29 May 2007). "Moscow Swelters in Heat Wave", Kommersant.com.	The temperature in Moscow reached +32.9 °C (91.2 °F) on 27 May. The Russian capital had not seen such a sustained heat wave for 128 years. On 28 May an absolute temperature record for May was set, breaking the record of +31.8 °C (89.2 °F) that had been registered back in 1891
2010	July	Eastern Europe, Russia heat wave	Barriopedro et al. 2011; Meshcherskaya et al. 2011; Mokhov 2011	Pakistan: all-time high of 53.7 C at Mohenjo-Daro, Sindh, May 26; Cold preceding winter in ETR (European Territory of Russia)–Cherenkova 2012
2012	summer	Drought and heat wave over Russia, Kazakhstan, Ukraine	http://theextinctionprotocol.wordpress.com/2012/07/31/severe-heatwave-drought-and-wildfires-destroy-russian-harvest/	Eurasian grain belt hit hard

List of Figures

Figure 1: Left panels: The mean June-July-August (JJA) precipitation variance from

MERRA, ERA-Interim, and NOAA-PRECL observations, computed for the period

1979-2012. Units are $(mm/day)^2$. A linear trend was removed for each calendar

month before computing the variances. Right panels: The same as the left, except

for the variance of the Ped (1975) drought index (see text).

Figure 2: Left panels: The mean JJA 2-meter temperature variance from MERRA, ERA-

Interim, and GHCN CAMS observations, computed for the period 1979-2012. Units

are $(°C)^2$. A linear trend was removed for each calendar month before computing the

variances. Right panels: The same as the left, except for the percent of the 2-meter

temperature variance explained by precipitation (see text).

Figure 3: The five leading Rotated Empirical Orthogonal Functions (REOFs) of the

combined monthly fields of 2-meter temperature and precipitation for JJA of 1979-

2012. The fields are normalized by their respective variances (standard deviation)

and a linear trend was removed for each calendar month before computing the

REOFs. The results are based on MERRA. Units are arbitrary.

Figure 4: The projection of the monthly JJA normalized 2-meter temperature and

precipitation fields onto the leading REOFs shown in Figure 3. The fields are not

detrended. The values are referred to in the text as the Rotated Principal

Components (RPCs). Units are arbitrary.

Figure 5: The standard deviation of the monthly JJA 2-meter temperature for the period 1980-2012. Units are °C. The top row is for MERRA, the second row is for GEOS-5 AGCM simulations with interactive land, the third row is for GEOS-5 AGCM simulations with disabled land-atmosphere feedback, the bottom row shows the difference between the second row and the third row, and indicates the effect of land-atmosphere.

Figure 6: The temporal correlation (shading) between the monthly JJA 250mb meridional wind (v) and leading RPCs of combined 2-meter temperature and precipitation for the period 1979-2012. A linear trend was removed for each calendar month before computing the covariances. Contours are the long-term mean JJA zonal wind (u) at 250mb (15, 20, 25 m/sec). Results are for MERRA.

Figure 7: Examples from MERRA of the 250mb v-wind anomalies (with respect to the 1980-2010 climatology) for selected months to highlight the predilection for Rossby wave structures similar to those shown in Figure 6 that are linked to monthly variability in surface meteorology. Units: m/sec.

Figure 8: The time evolution of the response of the eddy v-wind at σ=0.257 to an idealized constant vorticity source at 0°E, 50°N. The results are from a stationary wave model (Ting and Yu 1998) with a 3-dimensional JJA mean base state taken from MERRA for the period 1979-2010. The horizontal structure of the idealized forcing has a

sine-squared functional form, with horizontal scales of 10°longitude by 10°latitude and vertical profile (maximum of 5.6 x e^{-10} sec $^{-1}$ in the upper troposphere) following Liu et al (1998). See Schubert et al. (2011) for additional results. Contours are the long-term mean JJA zonal wind (u) at 250mb (15, 20, 25 m/sec) from MERRA.

Figure 9: The difference between the long term JJA means (1996-2011 minus 1980-1995) for 2-meter temperature (°C, left panels) and precipitation (mm/day, right panels). The top row is for MERRA, the second row is for ERA Interim, the third row is from GHCN_CAMS (for 2-meter temperature) and GPCP (for precipitation), and the bottom row is for the ensemble mean of the AMIP runs. Note the different shading intervals for the ensemble means.

Figure 10: Left panel: The linear trend in the annual mean SST from HadISST v1 (Rayner et al 2003) for the period 1980-2011. Right panel: The idealized SST forcing pattern that was used in the USCLIVAR drought working group to force various climate models. The pattern is composed of the three leading REOFs of the annual mean SST consisting of the cold phase of a Pacific decadal mode, the warm phase of an Atlantic Muli-decadal Oscillation (AMO) – like mode, and the trend pattern (see Schubert et al. 2009).

Figure 11: The JJA responses to the idealized SST forcing pattern shown in the right panel of Figure 10 averaged over four different AGCMs (CCM3, GEOS-5, GFS, and

GFDL). The top left panel is surface temperature (units: °C), the top right panel is

for precipitation (units: mm/day), and the bottom panel is for the 200mb height

(units: meters).

Figure 12: The time series of the 2-meter temperature anomalies for four different regions

across Eurasia. Top panels: Europe (10°W-30°E, 35°N-70°N); second from top:

European Russia (25°E-60°E, 46°N-62°N); second from bottom: South-central

Siberia (90°E-120°E, 45°N-65°N); bottom panels: Aral Sea region (45°E-75°E,

35°N-55°N). The left panels are from the CRUTEM4 data (1871-2010). The right

panels are based on the NOAA MLOST data (1880-2010). Units are °C.

Figure 13: The same as Figure 12, except for two of the 12 ensemble members of the

GEOS-5 AGCM simulations forced with observed SST and GHG forcings for the

period 1871-2010.

Figure 14: The correlation between the JJA mean surface temperature averaged over

European Russia (20°E-45°E, 52°N-65°N, indicated by the box), and the surface

temperature everywhere for the period 1901-1980. All data have a linear trend

removed at each grid point before computing the correlations. The top panel is for

the CRU TS3.0 observations. The middle panel is from the 12 GEOS-5 AMIP

simulations. Here the correlations are computed for each ensemble member

separately and then the correlations are averaged. The bottom panel is again for the

12 AMIP simulations, but here the correlations are based on the ensemble mean.

Figure 15: Results from one of the most extreme heat waves in European Russia found in the GEOSS-5 AGCM simulations (see text for details). The left panels show the evolution of the 2-meter temperature anomalies (°C) from the simulation for May through August of 2001 (anomalies are computed with respect to the 1980-2010 mean). The middle panels show the evolution of the 250mb v-wind (m/sec), and the right panels show the evolution of the surface soil wetness (dimensionless).

Figure 16: Results from an ensemble of 20 perturbation experiments initialized on 0Z May 15, 2001 for the ensemble member shown in Figure 15. The left panels show the original evolution of the 2-meter temperature (°C) from June through August of 2001 (a repeat of part of Fig. 15). The middle panels are the same as the left panels except for the ensemble mean of the perturbation runs, and the right panels are the same as the middle panels except for the ensemble mean surface soil wetness (dimensionless).

Figure 1: Left panels: The mean June-July-August (JJA) precipitation variance from MERRA, ERA-Interim, and NOAA-PRECL observations, computed for the period 1979-2012. Units are (mm/day)^2. A linear trend was removed for each calendar month before computing the variances. Right panels: The same as the left, except for the variance of the Ped (1975) drought index (see text).

Figure 2: Left panels: The mean JJA 2-meter temperature variance from MERRA, ERA-Interim, and GHCN CAMS observations, computed for the period 1979-2012. Units are (°C)^2. A linear trend was removed for each calendar month before computing the variances. Right panels: The same as the left, except for the percent of the 2-meter temperature variance explained by precipitation (see text)

Figure 3: The five leading Rotated Empirical Orthogonal Functions (REOFs) of the combined monthly fields of 2-meter temperature and precipitation for JJA of 1979-2012. The fields are normalized by their respective variances (standard deviation) and a linear trend was removed for each calendar month before computing the REOFs. The results are based on MERRA. Units are arbitrary.

89

Figure 4: The projection of the monthly JJA normalized 2-meter temperature and precipitation fields onto the leading REOFs shown in Figure 3. The fields are not detrended. The values are referred to in the text as the Rotated Principal Components (RPCs). Units are arbitrary.

Figure 5: The standard deviation of the monthly JJA 2-meter temperature for the period 1980-2012. Units are °C. The top row is for MERRA, the second row is for GEOS-5 AGCM simulations with interactive land, the third row is for GEOS-5 AGCM simulations with disabled land-atmosphere feedback, the bottom row shows the difference between the second row and the third row, and indicates the effect of land-atmosphere.

Figure 6: The temporal correlation (shading) between the monthly JJA 250mb meridional wind (v) and leading RPCs of combined 2-meter temperature and precipitation for the period 1979-2012. A linear trend was removed for each calendar month before computing the covariances. Contours are the long-term mean JJA zonal wind (u) at 250mb (15, 20, 25 m/sec). Results are for MERRA.

Figure 7: Examples from MERRA of the 250mb v-wind anomalies (with respect to the 1980-2010 climatology) for selected months to highlight the predilection for Rossby wave structures similar to those shown in Figure 6 that are linked to monthly variability in surface meteorology. Units: m/sec.

Figure 8: The time evolution of the response of the eddy v-wind at σ=0.257 to an idealized constant vorticity source at 0°E, 50°N. The results are from a stationary wave model (Ting and Yu 1998) with a 3-dimensional JJA mean base state taken from MERRA for the period 1979-2010. The horizontal structure of the idealized forcing has a sine-squared functional form, with horizontal scales of 10°longitude by 10°latitude and vertical profile (maximum of $5.6 \times e^{-10}$ sec^{-1} in the upper troposphere) following Liu et al (1998). See Schubert et al. (2011) for additional results. Contours are the long-term mean JJA zonal wind (u) at 250mb (15, 20, 25 m/sec) from MERRA

Figure 9: The difference between the long term JJA means (1996-2011 minus 1980-1995) for 2-meter temperature (°C, left panels) and precipitation (mm/day, right panels). The top row is for MERRA, the second row is for ERA Interim, the third row is from GHCN_CAMS (for 2-meter temperature) and GPCP (for precipitation), and the bottom row is for the ensemble mean of the AMIP runs. Note the different shading intervals for the ensemble means.

Figure 10: Left panel: The linear trend in the annual mean SST from HadISST v1 (Rayner et al 2003) for the period 1980-2011. Right panel: The idealized SST forcing pattern that was used in the USCLIVAR drought working group to force various climate models. The pattern is composed of the three leading REOFs of the annual mean SST consisting of the cold phase of a Pacific decadal mode, the warm phase of an Atlantic Muli-decadal Oscillation (AMO) – like mode, and the trend pattern (see Schubert et al. 2009).

Figure 11: The JJA responses to the idealized SST forcing pattern shown in the right panel of Figure 10 averaged over four different AGCMs (CCM3, GEOS-5, GFS, and GFDL).   The top left panel is surface temperature (units: °C), the top right panel is for precipitation (units: mm/day), and the bottom panel is for the 200mb height (units: meters).

Figure 12: The time series of the 2-meter temperature anomalies for four different regions across Eurasia. Top panels: Europe (10°W-30°E, 35°N-70°N); second from top: European Russia (25°E-60°E, 46°N-62°N); second from bottom: South-central Siberia (90°E-120°E, 45°N-65°N); bottom panels: Aral Sea region (45°E-75°E, 35°N-55°N). The left panels are from the CRUTEM4 data (1871-2010). The right panels are based on the NOAA MLOST data (1880-2010). Units are °C.
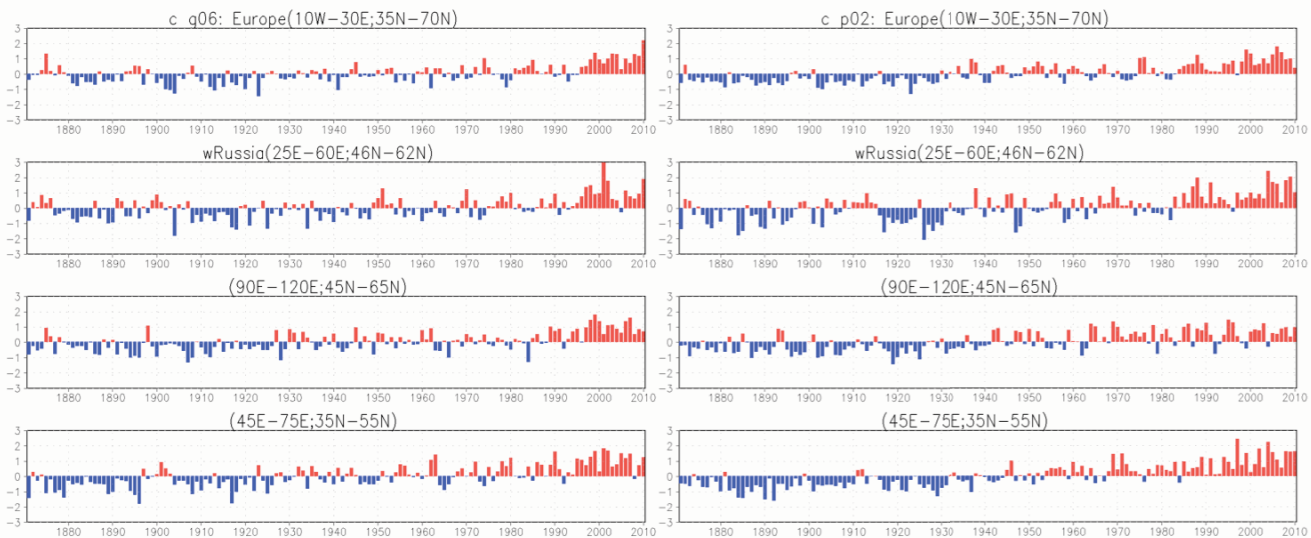
Figure 13: The same as Figure 12, except for two of the 12 ensemble members of the GEOS-5 AGCM simulations forced with observed SST and GHG forcings for the period 1871-2010.
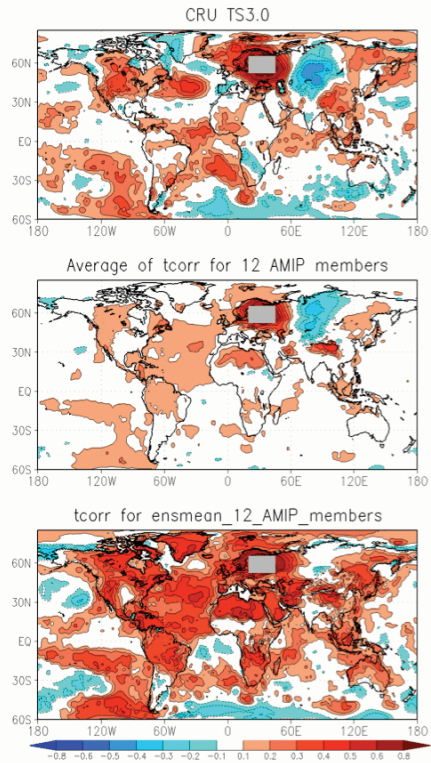
Figure 14: The correlation between the JJA mean surface temperature averaged over European Russia (20°E-45°E, 52°N-65°N, indicated by the box), and the surface temperature everywhere for the period 1901-1980. All data have a linear trend removed at each grid point before computing the correlations. The top panel is for the CRU TS3.0 observations. The middle panel is from the 12 GEOS-5 AMIP simulations. Here the correlations are computed for each ensemble member separately and then the correlations are averaged. The bottom panel is again for the 12 AMIP simulations, but here the correlations are based on the ensemble mean.
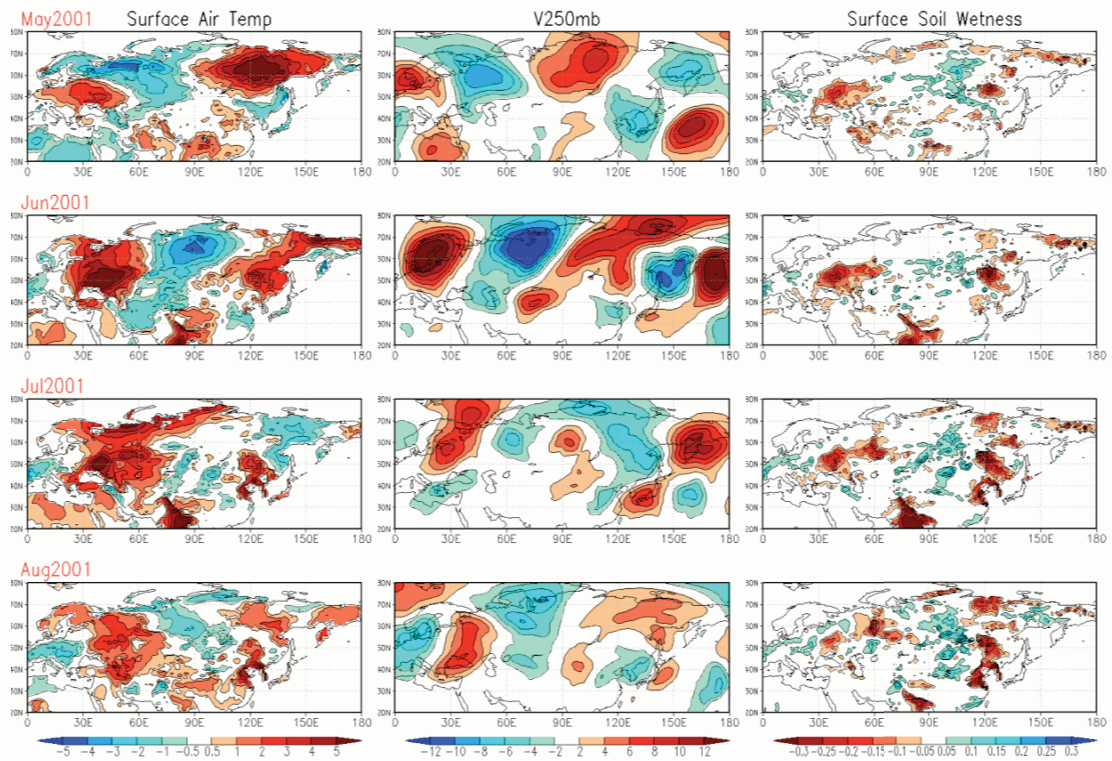
Figure 15: Results from one of the most extreme heat waves in European Russia found in the GEOSS-5 AGCM simulations (see text for details). The left panels show the evolution of the 2-meter temperature anomalies (°C) from the simulation for May through August of 2001 (anomalies are computed with respect to the 1980-2010 mean). The middle panels show the evolution of the 250mb v-wind (m/sec), and the right panels show the evolution of the surface soil wetness (dimensionless).
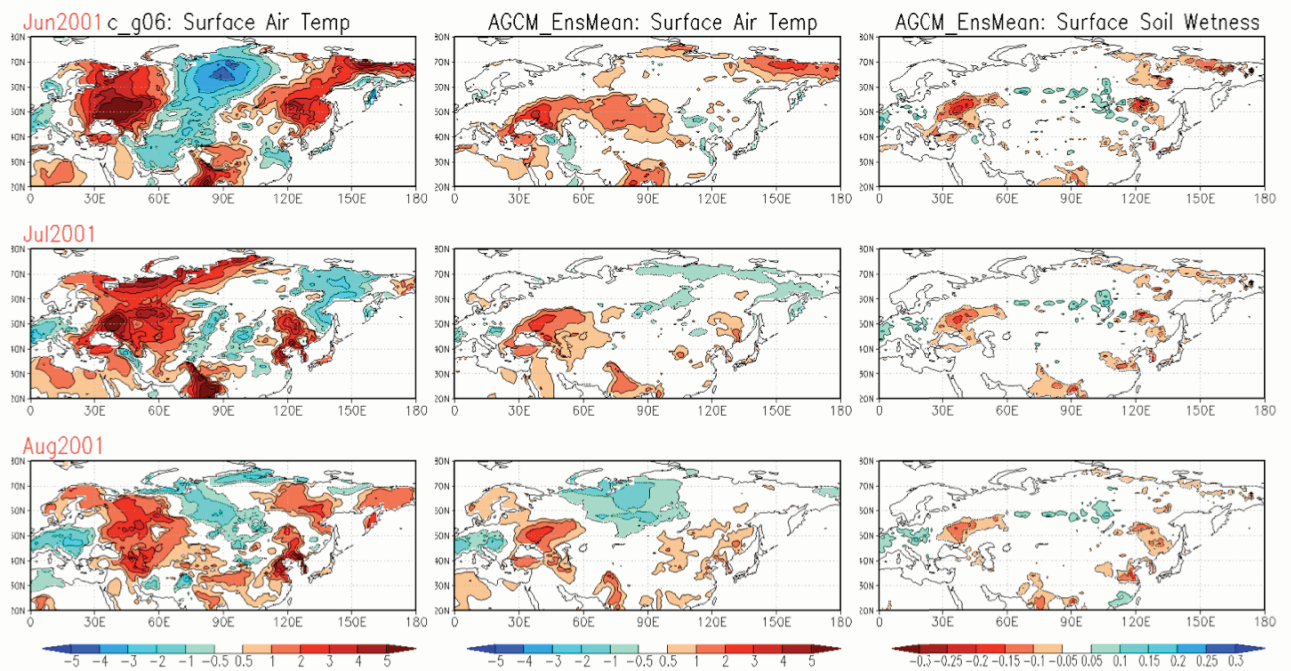
Figure 16: Results from an ensemble of 20 perturbation experiments initialized on 0Z May 15, 2001 for the ensemble member shown in Figure 15.   The left panels show the original evolution of the 2-meter temperature (°C) from June through August of 2001 (a repeat of part of Fig. 15). The middle panels are the same as the left panels except for the ensemble mean of the perturbation runs, and the right panels are the same as the middle panels except for the ensemble mean surface soil wetness (dimensionless).